Atypical protein kinase C induces cell transformation by disrupting Hippo/Yap signaling

Andrew Archibald[a,b], Maia Al-Masri[a,b], Alyson Liew-Spilger[a], and Luke McCaffrey[a,b,c]
[a]Rosalind and Morris Goodman Cancer Research Centre, [b]Division of Experimental Medicine, and [c]Department of Oncology, McGill University, Montreal, QC H3A 1A3, Canada

ABSTRACT **Epithelial cells are major sites of malignant transformation. Atypical protein kinase C (aPKC) isoforms are overexpressed and activated in many cancer types. Using normal, highly polarized epithelial cells (MDCK and NMuMG), we report that aPKC gain of function overcomes contact inhibited growth and is sufficient for a transformed epithelial phenotype. In 2D cultures, aPKC induced cells to grow as stratified epithelia, whereas cells grew as solid spheres of nonpolarized cells in 3D culture. aPKC associated with Mst1/2, which uncoupled Mst1/2 from Lats1/2 and promoted nuclear accumulation of Yap1. Of importance, Yap1 was necessary for aPKC-mediated overgrowth but did not restore cell polarity defects, indicating that the two are separable events. In MDCK cells, Yap1 was sequestered to cell–cell junctions by Amot, and aPKC overexpression resulted in loss of Amot expression and a spindle-like cell phenotype. Reexpression of Amot was sufficient to restore an epithelial cobblestone appearance, Yap1 localization, and growth control. In contrast, the effect of aPKC on Hippo/Yap signaling and overgrowth in NMuMG cells was independent of Amot. Finally, increased expression of aPKC in human cancers strongly correlated with increased nuclear accumulation of Yap1, indicating that the effect of aPKC on transformed growth by deregulating Hippo/Yap1 signaling may be clinically relevant.**

Monitoring Editor
Keith E. Mostov
University of California, San Francisco

Received: May 6, 2015
Revised: Aug 6, 2015
Accepted: Aug 7, 2015

INTRODUCTION

Cancer is a leading cause of mortality, and epithelial cells are the origin for malignant transformation in >80% of cancers (Dimri *et al.*, 2005). The acquisition of a malignant phenotype involves loss of apical-basal cell polarity, epithelial reorganization, and loss of growth control, which ultimately compromises tissue structure and function. Apical-basal polarity is a fundamental property of epithelial cells and organizes intracellular signaling complexes; disrupted polarity can alter cell signaling to promote cancer progression (Martin-Belmonte and Perez-Moreno, 2011; Halaoui and McCaffrey, 2014).

Atypical protein kinase C (aPKC) isoforms (ι/λ and ζ) share >73% sequence identity and are frequently activated and up-regulated in cancer types, including lung, ovarian, breast, prostate, liver, bladder, head and neck, pancreas, and skin (Tsai *et al.*, 2000; Langzam *et al.*, 2001; Evans *et al.*, 2003; Eder *et al.*, 2005; Regala *et al.*, 2005; Cohen *et al.*, 2006; Kojima *et al.*, 2008; Du *et al.*, 2009; Yao *et al.*, 2010, 2012; Lin *et al.*, 2012; McCaffrey *et al.*, 2012; Atwood *et al.*, 2013; Kato *et al.*, 2013; Linch *et al.*, 2014; Paul *et al.*, 2014; Yin *et al.*, 2014). An oncogenic role for aPKC is supported by studies showing that knockdown or inhibition of aPKC impairs growth of human cancer cell lines or epithelial cells overexpressing H-Ras, v-Src, c-Raf, ErbB2, or PI3K (Yao *et al.*, 2010; Paget *et al.*, 2011; Linch *et al.*, 2014). Moreover, reducing aPKC partially restores polarity in H-Ras– and ErbB2-transformed epithelial cells, indicating that aPKC is required downstream of strong oncogenes for loss of polarity (Aranda *et al.*, 2006; Linch *et al.*, 2014). Therefore aPKC is required downstream of multiple established oncogenes, but the direct potential role of aPKC in cell transformation is unclear.

This article was published online ahead of print in MBoC in Press (http://www.molbiolcell.org/cgi/doi/10.1091/mbc.E15-05-0265) on August 12, 2015.

Address correspondence to: Luke McCaffrey (luke.mccaffrey@mcgill.ca).

Abbreviations used: AIP4, atrophin interacting protein 4; Amot, angiomotin; aPKC, atypical protein kinase C; Bad, Bcl-2–associated death promoter; Crb3, Crumbs homologue 3, ErbB2, epidermal growth factor receptor II; ERK1/2, extracellular signal-regulated kinase; Hpo, Hippo; Lats1/2, large tumor suppressor; Lgl, lethal giant larvae, MDCK, Madin–Darby canine kidney; Mst1/2, mammalian STE20-like protein kinase; NF-κB, nuclear factor κ-light-chain enhancer of activated B cells; NMuMGs, normal murine mammary epithelial cells; PDK-1, 3-phosphoinositide–dependent protein kinase-1, PI3K, phosphoinositol 3-kinase; PIK-3CA, PI3K catalytic alpha polypeptide; PTEN, phosphatase and tensin homologue; Rac1, Ras-related C3 botulinum toxin substrate; Raf, rapidly accelerated fibrosarcoma, RASSF1, Ras-associated factor; Sav1, salvador homologue; Scrib, Scribble; Src, Rous sarcoma oncogene cellular homologue; Stat3, signal transducers and activators of transcription, Taz1, transcriptional coactivator with PDZ-binding motif (TAZ); Yap, Yes-associated protein 1; Yki, Yorkie; ZO-1, zona occludens.

aPKC exists in an autoinhibited state in which a pseudosubstrate peptide motif acts as an internal competitive inhibitor that is regulated by protein–protein interactions (Graybill *et al.*, 2012). aPKC activation requires direct phosphorylation by PDK-1 on threonine 410 within the activation loop, which is dependent on upstream PI 3-kinase (PI3K) to activate PDK-1 (Chou *et al.*, 1998). aPKC has been shown to function downstream of PI3K/PDK-1 in human cancer cell lines. For example, silencing aPKC in tumor cell lines with high PI3K or low PTEN suppresses growth by inducing senescence (Paget *et al.*, 2011). Moreover, a PI3K/PDK-1/aPKC pathway inhibits apoptosis in cancer cells through direct phosphorylation of the proapoptotic protein Bad by aPKC, and inhibiting PI3K blocks aPKC activity and Bad phosphorylation (Desai *et al.*, 2011). Of interest, the aPKCι gene resides on chromosome 3q26, one of the most highly amplified regions in cancers, a region that also includes the gene for PIK3CA, which encodes the p110α subunit of PI3K (Fields *et al.*, 2007; Yang *et al.*, 2008; Justilien *et al.*, 2014). This therefore provides a mechanism by which aPKC may be overexpressed and activated by PI3K in some cancers.

In normal polarized epithelial cells, aPKC resides at tight junctions and the apical membrane in complex with the apical Par and Crumbs polarity complexes, but it is mislocalized from the plasma membrane to the cytoplasm in tumor cells (Grifoni *et al.*, 2007; Kojima *et al.*, 2008; Du *et al.*, 2009; Martin-Belmonte and Perez-Moreno, 2011; Halaoui and McCaffrey, 2014). aPKC functions to establish apical-basal polarity by specifying apical membrane identity and suppressing basolateral identity. This polarized architecture permits the assembly of signaling networks that appropriately interpret the cellular environment, and disrupted aPKC polarity can affect key signaling mediators involved in tumor growth and invasion, including Ras, NF-κB, Stat3, ERK1/2, and Rac1 (Sanz *et al.*, 1999; Justilien and Fields, 2009; Iden *et al.*, 2012; McCaffrey *et al.*, 2012; Atwood *et al.*, 2013; Halaoui and McCaffrey, 2014; Paul *et al.*, 2014).

Epithelial cells exhibit contact-inhibited growth, which depends on cell density constraints, rather than cell–cell contact (Puliafito *et al.*, 2012; Eisenhoffer and Rosenblatt, 2013). The Hippo/Yap signaling pathway has emerged as a central regulator of epithelial growth control. Numerous inputs have been identified that can regulate Hippo signaling, including the actin cytoskeleton, extracellular matrix stiffness, cell adhesion, cell polarity, and G protein–coupled receptors (Yu and Guan, 2013). The canonical Hippo pathway involves upstream Mst1/2, which phosphorylates and activates Lats1/2, which can phosphorylate Yap1 to stimulate cytoplasmic sequestration and exclusion from the nucleus (Yu and Guan, 2013). Mst1/2 and Lats1/2 can be recruited to the plasma membrane independently, where they couple for Lats1/2 phosphorylation by Mst1/2. It has been reported that Lats1/2 associates with NF2/Merlin for membrane recruitment (Yin *et al.*, 2013), whereas Mst1/2 binds the scaffold Sav1, which is required for membrane recruitment and subsequent phosphorylation of Lats1/2 (Yu and Guan, 2013). The Hippo pathway can also be regulated by cell polarity. For example, Crumbs 3 can sequester Yap1, and Scrib can act as a scaffold for Mst1/2, Lats1/2, and Taz, and disruption of these polarity complexes enables nuclear translocation of Yap1/Taz and epithelial overgrowth (Varelas *et al.*, 2010; Cordenonsi *et al.*, 2011).

Angiomotin (Amot) is a scaffold protein that regulates the actin cytoskeleton and cell proliferation. The N-terminal domain of Amot interacts with Yap1, which sequesters it to tight junctions and suppresses epithelial cell proliferation and tumorigenesis, whereas an isoform lacking the N-terminal domain does not regulate actin or Yap1 (Zhao *et al.*, 2011; Yi *et al.*, 2013). The relationship between Amot and Lats1/2 is complex; through a scaffolding function, Amot can associate with and promote Lats1/2 activity and subsequent Yap1 phosphorylation (Paramasivam *et al.*, 2011). Conversely, Lats1/2 phosphorylates Amot to recruit AIP4, which ubiquitinates and protects Amot from degradation (Adler *et al.*, 2013).

The Hippo/Yap pathway is frequently disrupted in cancers, and up-regulation or nuclear accumulation of Yap1/Taz has been reported in numerous cancer types, including lung, ovarian, breast, liver, esophageal, cervical, and gastric (Ma *et al.*, 2014). Moreover, a high level of Yap1/Taz is associated with increased invasiveness, metastasis, cancer stem cell phenotypes, and poor patient outcomes (Ma *et al.*, 2014). Because of its inhibitory role in Yap1/Taz activity, the Hippo pathway is a tumor suppressor pathway. Down-regulation of Mst is observed in some cancers, and deletion of both of Mst1 and Mst2 in mice causes liver and colon tumors and dysplasia in the intestine (Ma *et al.*, 2014). Down-regulation of Lats1/2 expression or activity is also observed in some cancers (Ma *et al.*, 2014). However, mutations of Mst and Lats kinases are rare in common cancers, indicating that additional mechanisms contribute to deactivation of the Hippo pathway (Romano *et al.*, 2014).

Although aPKC is activated and overexpressed in multiple cancers, the role of aPKC gain of function on cell transformation of polarized epithelia is not understood. Here we investigate the consequence of expression of activated aPKC in normal epithelial cells and find that it is sufficient to induce a transformed phenotype caused in part by disruption of Hippo signaling.

RESULTS

aPKC gain of function induces cell transformation of epithelial cells

To investigate the consequence of aPKC gain of function on epithelial cells, we stably expressed green fluorescent protein (GFP; control) or a constitutively active form of aPKCζ in which Thr-410 was substituted with Glu (T410E; aPKCζ-ca; Standaert *et al.*, 1999) in Madin–Darby canine kidney (MDCK) cells (Figure 1A). MDCK cells are a well-characterized cell model that exhibits contact-inhibited growth and achieves a highly polarized state. They are therefore ideal for understanding mechanisms of contact inhibition and cell transformation (Puliafito *et al.*, 2012). When grown in two-dimensional (2D) cultures, control cells grew as a uniform monolayer with a cobblestone appearance, typical of polarized epithelia. However, aPKCζ-ca–expressing cells exhibited a spindle-like phenotype that grew as stratified epithelial layers (Figure 1, B–D). To quantify the cell shape changes, we stained cells with phalloidin to label F-actin and measured the elongation factor, defined here as the ratio of the long to the short axis. Whereas GFP control cells had an elongation factor of ~1.5, aPKCζ-ca–expressing cells were significantly stretched and had an elongation factor of almost 4 (Figure 1C). We next examined the effect of aPKCζ-ca expression in three-dimensional (3D) epithelial cell cultures. Single-cell suspensions were seeded onto basement membrane–coated dishes and allowed to grow for 7 d into multicellular 3D structures. Remarkably, cells expressing aPKCζ-ca formed 3D structures that were more than twofold larger than GFP-expressing controls (Figure 1, E and F). To further examine growth kinetics, we imaged 3D cell cultures at 1-h intervals for 151 h (Supplemental Figure S1A and Supplemental Videos S1 and S2). The time to reach half-maximal size ($t_{1/2}$) was 67 ± 2 h for control and 95 ± 3 h for aPKCζ-ca structures, and aPKCζ-ca structures had a growth rate twice that of GFP controls at $t_{1/2}$ (44 ± 4 vs. 18 ± 1 μm^2/h). To determine whether overgrowth was associated with changes in proliferation or apoptosis, we stained 3D cultures for Ki67 and cleaved caspase 3, respectively. The proportion of Ki67-positive aPKCζ-ca cells was substantially higher than in control cells (37 vs. 21%; Figure 1, G and H). In addition, there was a

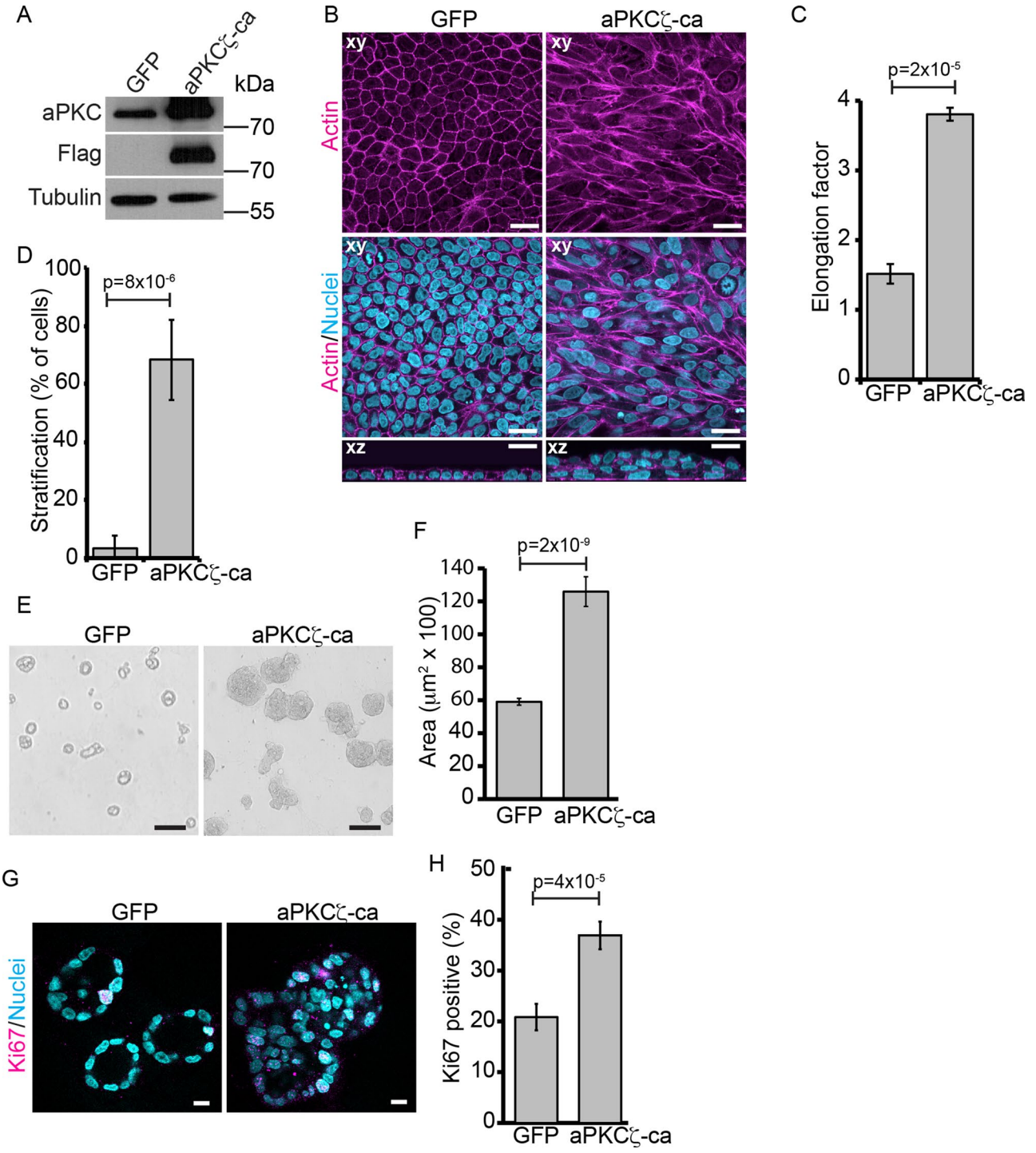

FIGURE 1: aPKC induces epithelial overgrowth in 2D and 3D cultures. (A) Immunoblot showing aPKC expression in MDCK cells expressing GFP (control) or FLAG-tagged aPKC-ca. (B) Cells expressing GFP or aPKCζ-ca were grown to confluence as 2D cultures and stained with phalloidin to label F-actin. Bottom, *xz*-projections derived from *z*-stacks. (C) Quantification of elongation factor (long axis/short axis). Three fields/triplicate experiment. (D) Quantification of cell stratification (≥2 cells stacked in the *z*-axis). Five fields/duplicate experiment. (E) Phase contrast images showing GFP- and aPKCζ-ca–expressing cells grown in 3D culture. (F) Quantification of the size of each structure. We measured 511 GFP and 844 aPKCζ-ca structures. (G) The 3D structures were immmunostained for Ki67. (H) Quantification of the percentage of Ki67-positive cells. We measured 671 GFP and 1568 aPKCζ-ca structures. Error bars, SD. The *p* values were calculated using the Student's *t* test. Bars, 10 μm (B, G) and 100 μm (E).

modest but significant increase in the proportion of apoptotic cells in aPKCζ-ca 3D culture compared with GFP controls (3.5 vs. 7%; Supplemental Figure S1, B and C). Furthermore, we found that overexpression of constitutively active aPKCι or wild-type aPKCζ and aPKCι was also capable of inducing overgrowth of 3D MDCK cysts (Supplemental Figure S1, D and E). To determine whether expression

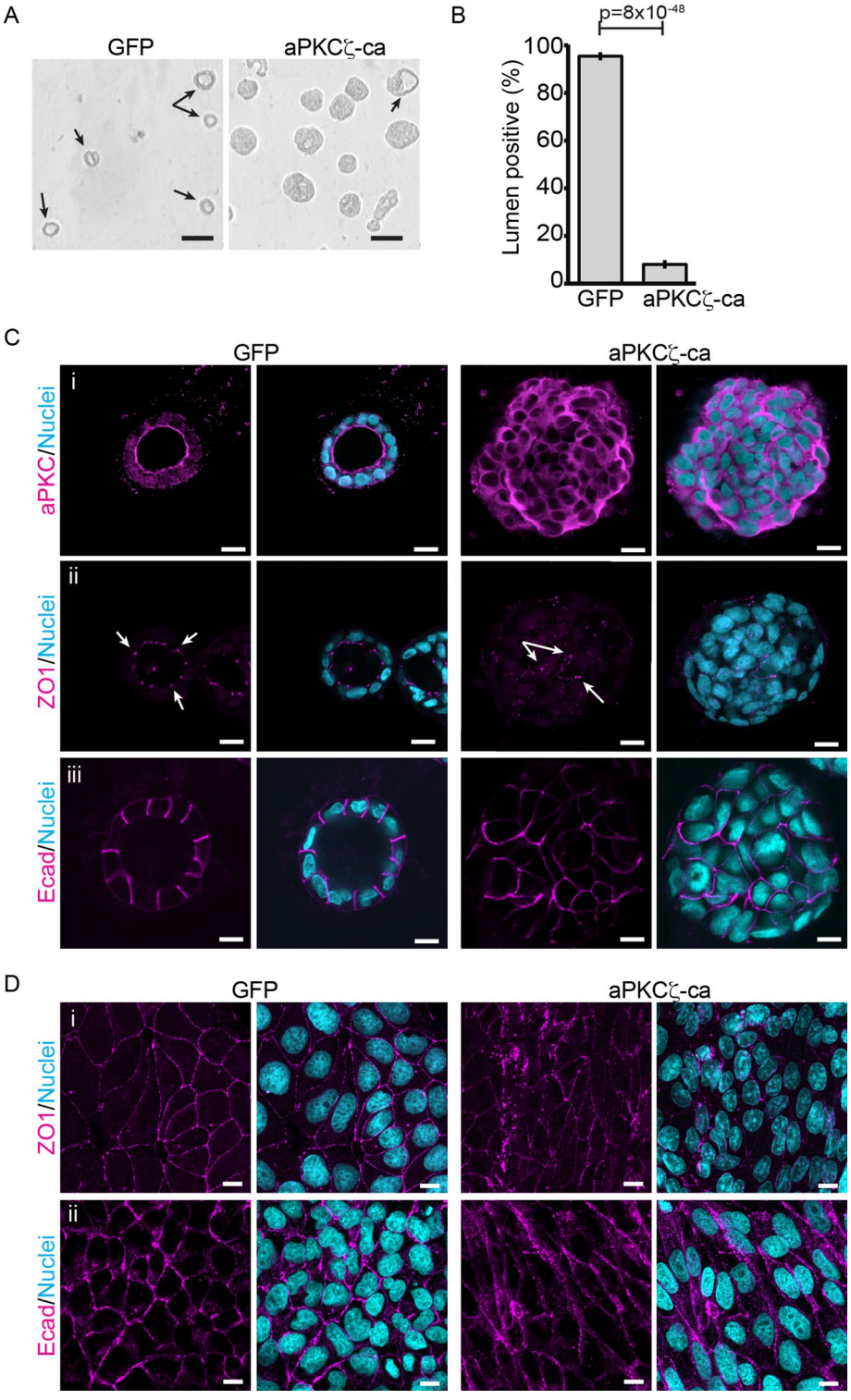

FIGURE 2: aPKCζ-ca expression disrupts cell polarity. (A) Phase contrast images showing GFP- (control) and aPKCζ-ca–expressing cells grown in 3D culture. Arrows show structures with luminal cavities. (B) Quantification of percentage of 3D structures with a visible lumen. We measured 501 control and 900 aPKCζ-ca structures. Error bars, SD. The *p* value was calculated using the Student's *t* test. (C) Immunofluorescence images showing GFP and aPKCζ-ca MDCK cells from 3D cultures immunostained for aPKC (i), ZO-1 (ii), and E-cadherin (iii). Arrows show examples of ZO-1–positive foci. (D) MDCK cells were grown to confluence in 2D culture and immunostained for ZO-1 (i) and E-cadherin (ii). Bars, 100 μm (A), 10 μm (C, D).

of aPKC was sufficient to induce epithelial overgrowth in other epithelial cell types, we expressed aPKCζ-ca in normal murine mammary epithelial cells (NMuMGs). Similar to MDCK cells, expression of PKCζ-ca caused multilayered growth in 2D cultures and a six-fold increase in size of 3D cultures (Supplemental Figure S1, F–H). However, aPKCζ-ca did not affect cell shape in NMuMG cells, indicating that epithelial stratification and epithelial overgrowth was not dependent on cell shape changes. Collectively these data demonstrate that aPKCζ-ca induces loss of epithelial growth control in both 2D and 3D culture environments.

aPKC-ca expression prevents the establishment of apical-basal polarity

Luminal filling and loss of apical-basal polarity are characteristics of transformed cells in developing cancers. Depletion of aPKC or other members of the Par complex (Par3 and Par6) in 3D cultures results in structures that form multiple lumens instead of a single lumen but nonetheless retain apical-basal polarity (Jaffe *et al.*, 2008; Hao *et al.*, 2010; Durgan *et al.*, 2011). We therefore examined whether aPKC gain of function would affect lumen formation or apical-basal polarity in 3D culture. Whereas >90% of control MDCK cells form 3D structures with a central lumen, <10% of aPKCζ-ca cells had a prominent lumen (Figure 2, A and B). In normal epithelia, aPKC is localized to the apical membrane, but it is mislocalized to the cytoplasm in tumors (Grifoni *et al.*, 2007; Kojima *et al.*, 2008; Du *et al.*, 2009). We therefore examined the localization of aPKC in 3D cultures and found that, similar to aPKC localization in human tumors, total aPKC was cytoplasmic (Figure 2C). To determine further whether cells fail to polarize or if instead form microlumen, we examined the localization of several adhesion and apical polarity markers. In control 3D structures F-actin, ezrin, and Par6 are enriched at the apical membrane and mark the lumen. In contrast, aPKCζ-ca 3D structures were solid and did not form detectable microlumen (Supplemental Figure S2A and Supplemental Videos S3 and S4). In GFP control 3D structures, ZO-1 localized at tight junction foci located apically, and E-cadherin localized basolaterally. In aPKCζ-ca 3D structures, E-cadherin localized around cells and, surprisingly, although cells lack apical-basal polarity, ZO-1–positive foci were detected, indicating that cells may be

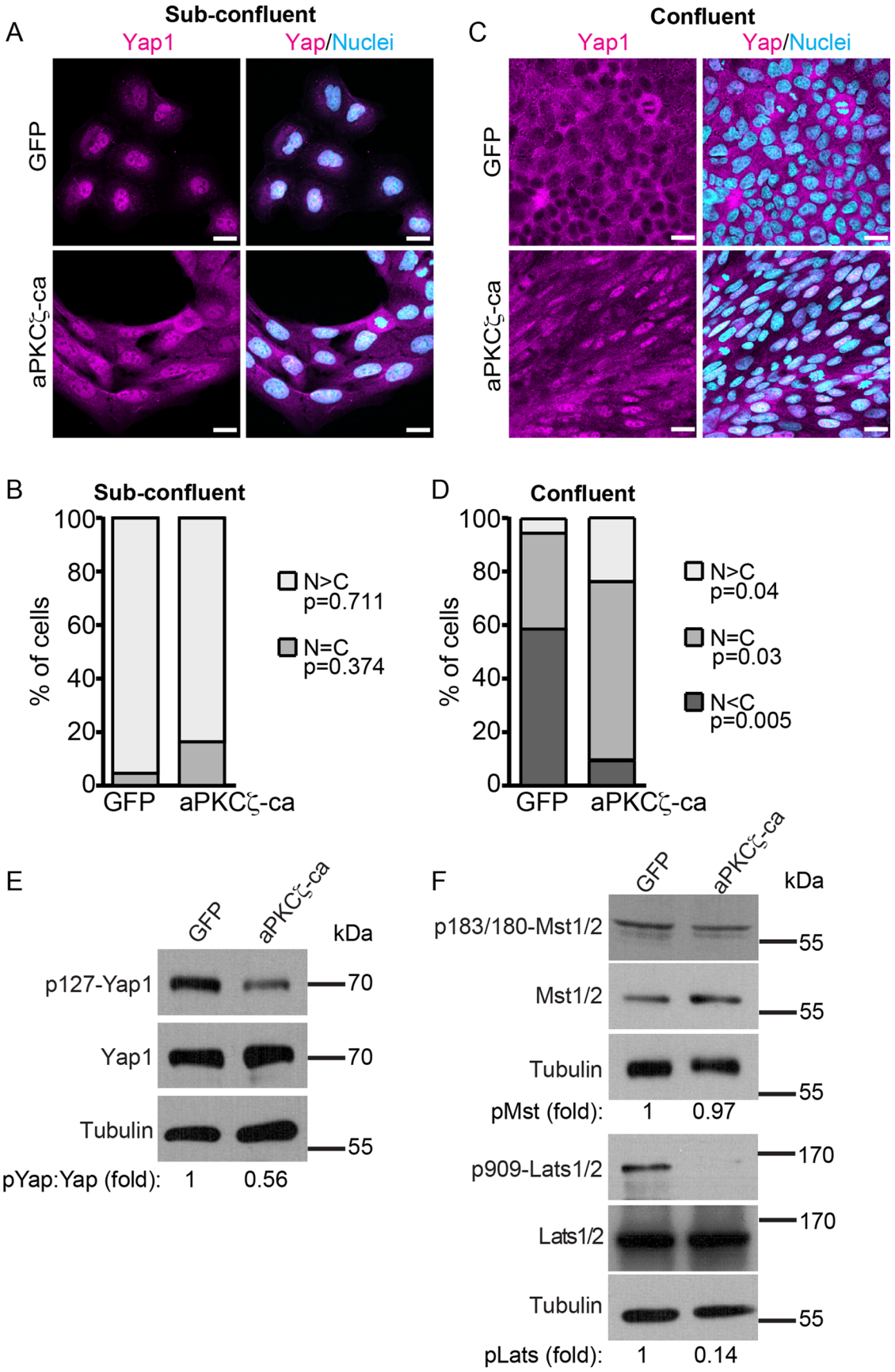

FIGURE 3: aPKCζ-ca expression alters the activity of the Hippo pathway. (A) Immunofluorescence images showing GFP (control) and aPKCζ-ca MDCK cells grown as subconfluent cultures and immunostained for Yap1. (B) Quantification of the nuclear/cytoplasmic localization of Yap1 from cultures shown in A. Cells were scored as nuclear

able to form tight junctions, at least to a limited degree (Figure 2C). We also stained for Numb, a basolateral protein that can bind E-cadherin and is excluded from the membrane by aPKC-dependent phosphorylation (Nishimura and Kaibuchi, 2007; Smith *et al.*, 2007). Whereas Numb was localized basolaterally in control 3D structures, it was diffuse in cells from aPKCζ-ca–expressing spheres (Supplemental Figure S2A), consistent with delocalized aPKC activity.

In 2D cultures, E-cadherin and ZO-1 were localized to cell membrane in both GFP control and aPKCζ-ca MDCK cells, whereas Par6 was mislocalized in aPKCζ-ca cells (Figure 2D and Supplemental Figure S2B). Collectively these results demonstrate that aPKC gain of function causes loss of apical-basal polarity, disrupts epithelial organization, and impairs growth control, which are key features of cell transformation.

aPKC suppresses Hippo signaling and induces nuclear accumulation of Yap1

The transcriptional coregulator Yap1 is an important regulator of epithelial homeostasis and is excluded from the nucleus by multiple mechanisms, including those that depend on cell density and polarity (Varelas *et al.*, 2010). Because aPKCζ-ca induced loss of apical-basal polarity and epithelial growth control, we asked whether aPKCζ-ca affected Hippo/Yap1 signaling. In subconfluent control MDCK cultures, Yap1 is predominantly nuclear, whereas in confluent monolayers, Yap1 is excluded from the nucleus. In contrast, Yap1 is predominantly nuclear in both subconfluent and confluent cultures of aPKCζ-ca–expressing cells (Figure 3, A–D), consistent with a role for aPKCζ-ca in causing epithelial overgrowth. A similar aPKC-dependent relocalization of Yap1 to the nucleus was observed in NMuMG cells (Supplemental Figure S3, A and B).

The nuclear–cytoplasmic localization of Yap1 is controlled by phosphorylation on Ser-127 by Lats1/2 (Yu and Guan, 2013). Consistent with a role for aPKC in regulating Yap1 subcellular localization, we found that aPKCζ-ca cells had reduced levels of pS127-Yap1, with no change in total Yap1 expression (Figure 3E). Because the Hippo pathway can regulate Yap1 phosphorylation, we next asked whether reduced Yap1 phosphorylation reflected altered Mst1/2 and Lats1/2 activity. Phosphorylation of Mst1/2 on Thr-183/Thr-180 and Lats1/2 on Ser-909 is essential for their kinase activity, and phosphorylation of these sites can be used as an indication of activity (Glantschnig *et al.*, 2002; Chan *et al.*, 2005). Whereas there was no change in the phosphorylation of Mst1/2 on Thr-183/Thr-180, Lats1/2 phosphorylation on Ser-909 was dramatically reduced in aPKCζ-ca MDCK cells compared with the GFP control (Figure 3F). A reduction in Lats1/2 phosphorylation was also observed in NMuMG cells (Supplemental Figure S3C), indicating that aPKCζ gain of function negatively regulates the Hippo pathway and induces accumulation of Yap1 in the nucleus of epithelial cells.

Yap1 overexpression affects epithelial growth but not apical-basal polarity

We demonstrated that aPKCζ gain of function resulted in loss of epithelial growth control and elevated nuclear Yap1. Of interest, it was reported that Yap1 expression induces transformation and stratification in MDCK cells grown in 2D culture (Zhao *et al.*, 2011), but the consequence of Yap1 expression in 3D culture is not clear. Therefore we further investigated the effect of Yap1 overexpression in MDCK cells (Supplemental Figure S4, A and B). In 2D cultures, we confirmed that Yap1 expression induced stratification, although the effect was weak (Supplemental Figure S4, C and D). Furthermore, we observed that similar to GFP control cells, Yap1-overexpressing cells retained a cobblestone appearance (Supplemental Figure S4, C and E), indicating that stratification is not a consequence of cell shape changes. In 3D culture, Yap1 induced approximately twofold increase in the size of 3D structures compared with the control (Supplemental Figure S4, F and G). Furthermore, 3D structures overexpressing Yap1 were able to polarize and form a lumen; however, we observed approximately threefold increase in the proportion of multiluminal structures (Supplemental Figure S4, H–J). Moreover, Yap1 expression increased the proportion of cells expressing the proliferation marker Ki67 but had no effect on cleaved caspase 3 (Supplemental Figure S4, K–N), indicating that Yap1 affects proliferation to induce epithelial overgrowth. Therefore overexpression of Yap1 is sufficient to induce epithelial overgrowth but does not dramatically affect cell shape or ablate apical-basal polarity.

aPKC gain of function depends on Yap1 for epithelial overgrowth

Our data suggest that Yap1 may be responsible for aPKC-induced epithelial overgrowth. To test this possibility, we examined whether disrupting Yap1 expression or function would affect aPKCζ-ca–induced epithelial overgrowth. We identified two shYap1 constructs that efficiently knocked down Yap1 in MDCK cells (Supplemental Figure S5A). In 2D culture, knockdown of Yap1 did not affect epithelial organization of control cells and did not rescue the spindly phenotype of aPKCζ-ca cells (Supplemental Figure S5, B and C). However, depletion of Yap1 did reduce the formation of stratified epithelia induced by aPKCζ-ca expression (Supplemental Figure S5, D and E). These results are consistent with our earlier experiments indicating that Yap1 is involved in stratified overgrowth but not cell shape.

In 3D cultures, expression of shYap1 significantly reduced aPKC-mediated epithelial overgrowth (Figure 4, A and B). Knockdown of Yap1 had little effect on the growth of GFP control 3D structures, indicating that Yap1 may not been essential for growth under basal conditions or that residual Yap1 is sufficient for normal growth. Finally, depleting Yap1 did not affect lumen formation in GFP control 3D structures and did not rescue loss of apical-basal polarity in aPKCζ-ca 3D structures (Supplemental Figure S5F and Supplemental Videos S5 and S6), supporting our earlier data that Yap1 does not regulate apical-basal polarity in these cells.

As a complementary approach to evaluate whether Yap1 is required for overgrowth of aPKCζ-ca 3D structures, we expressed a dominant-negative form of Yap1 (dnYap1) that retains binding to transcriptional cofactors but lacks the transactivation domain and therefore blocks Yap1-dependent transcription (Cao *et al.*, 2008). Similar to knockdown of Yap1, expression of dnYap1 rescued epithelial overgrowth of aPKCζ-ca 3D structures (Figure 4, C and D).

enriched (N > C), equal nuclear/cytoplasmic (N = C), or nuclear depleted (N < C). Three independent fields/duplicate experiment. (C) Immunofluorescence images showing MDCK cells grown as confluent cultures and immunostained for Yap1. (D) Quantification of the nuclear/cytoplasmic localization of Yap1 from cultures shown in C. Three independent fields/duplicate experiment. (E) Immunoblot of lysates from confluent cells for phosphorylated Ser127-Yap1 (p127-Yap1) and total Yap1. (F) Immunoblot of lysates from confluent cells for phosphorylated Thr183/Thr180-Mst1/2 (p183/180-Mst1/2), total Mst1/2, phosphorylated Ser909-Lats1/2 (p909-Lats1/2), and total Lats1/2. Fold changes in protein were determined from four blots. Bars, 10 μm. Error bars, SD. The *p* values were calculated using the Student's *t* test.

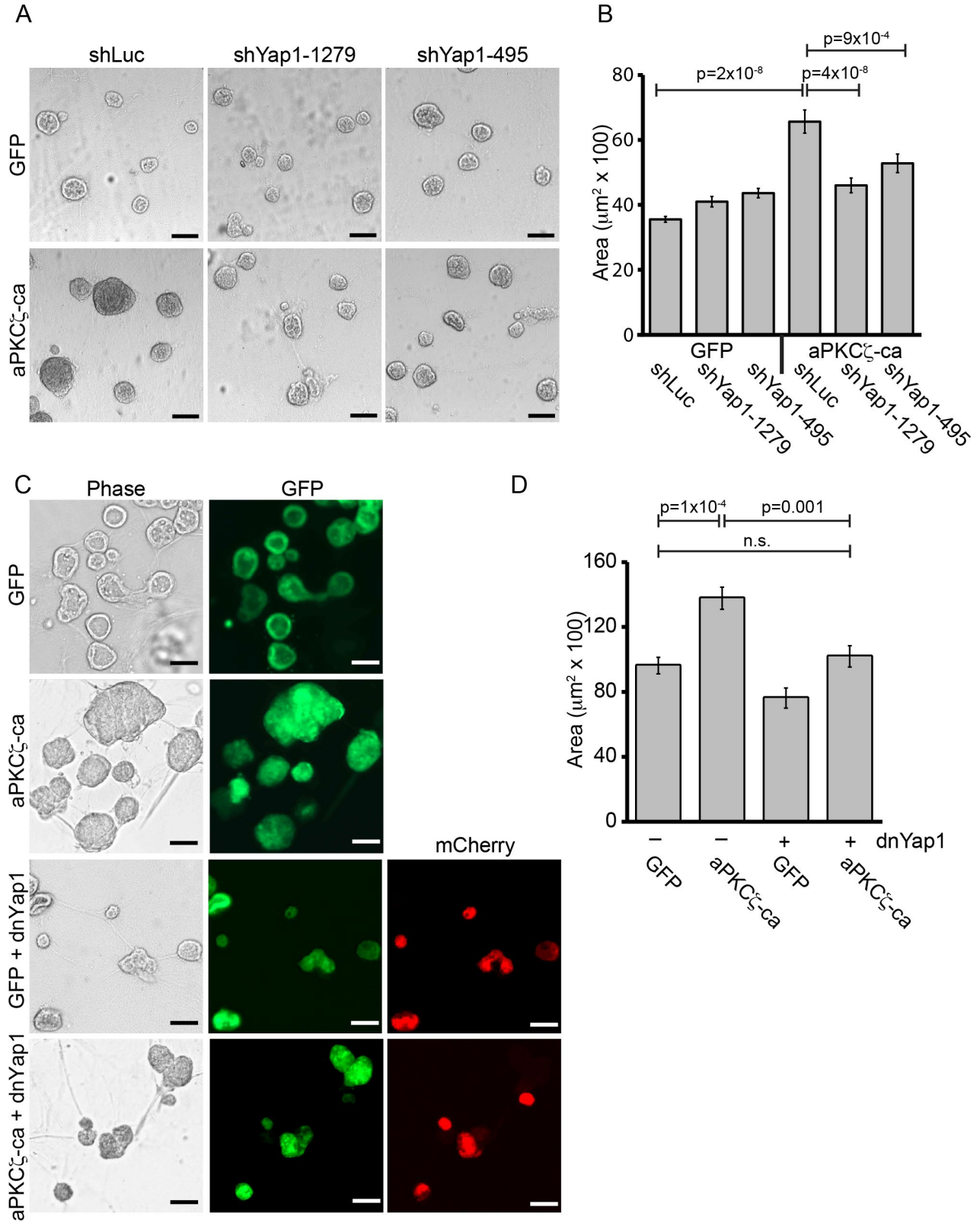

FIGURE 4: Yap1 is required for aPKCζ-ca loss of growth control. (A) Phase contrast images of 3D structures from GFP- (control) and aPKCζ-ca–expressing MDCK cells coexpressing control short hairpin RNA (shRNA; shLuc) or Yap1-specific shRNAs (shYap1-1279 and shYap1-495). (B) Quantification of the size of 3D structures. We measured 143 structures/condition. (C) Phase contrast and direct fluorescence images of 3D structures from GFP and aPKCζ-ca cells expressing dominant-negative Yap1 (dnYap1). GFP and aPKCζ-ca cells are marked by GFP expression, and dnYap1 cells are marked by mCherry expression. (D) Quantification of the size of 3D structures. We measured 325 GFP, 238 aPKCζ-ca, 79 GFP+dnYap1, and 90 aPKC+dnYap1 structures. Bars, 100 μm. Error bars, SD. The *p* values were calculated using one-way ANOVA and Tukey honest significant difference (HSD) post hoc tests.

Collectively these data support a role for Yap1 downstream of aPKCζ-ca, which regulates loss of growth control induced by aPKC but does not affect apical-basal polarity.

aPKC gain of function disrupts Mst1/2 localization to cell junctions

Our foregoing observations show that aPKCζ-ca expression causes a dramatic reduction in the phosphorylation of Lats1/2 at Ser-909, whereas Mst1/2 activity is unaffected. This was unexpected because it was reported that phosphorylation of Lats1/2 on Ser-909 was dependent on Mst1/2 activity (Chan *et al.*, 2005). This led us to hypothesize that aPKCζ-ca uncouples Mst1/2 from Lats1/2 through a mechanism other than reduced Mst1/2 activity. We therefore examined whether the association between Mst1/2 and Lats1/2 was affected by aPKC expression. Indeed, we observed reduced interaction between Mst1/2 and Lats1/2 in aPKCζ-ca cells relative to GFP control cells (Figure 5A). It was suggested that Mst1/2 is recruited to the plasma membrane, which enables the coupling with Lats1/2 to regulate downstream Yap1 function (Yin *et al.*, 2013). We therefore examined whether aPKCζ-ca affected Mst1/2 localization to the plasma membrane. Using two independent antibodies, we detected Mst1/2 at cell junctions in GFP control cells; however, it is diffuse in aPKCζ-ca cells (Figure 5B and Supplemental Figure S6A). Membrane recruitment and coupling of Mst1/2 to Lats1/2 have been reported to require the adaptor protein Sav1 (Avruch *et al.*, 2012; Yin *et al.*, 2013). We therefore examined whether Sav1 localization was also affected by aPKCζ-ca. We observed that Sav1 was mislocalized from the junctions in 2D aPKCζ-ca cells and the apical membrane in 3D cultures (Figure 5B and Supplemental Figure S6E). We next examined whether aPKC might disrupt the Mst/Sav1 complex, which could account for their mislocalization. However, coimmunoprecipitation experiments indicated that Sav1 still associated with Mst1/2 in aPKCζ-ca cells (Supplemental Figure S6B). Because aPKC affected the localization of Mst1/2 and Sav1 but not their interaction, we tested whether aPKC was part of a complex with Mst1/2 and Sav1, which could contribute to their altered localization. Indeed, we found that both Mst1/2 and Sav1 were coimmunoprecipitated with aPKCζ-ca, whereas Lats1/2 was not (Figure 5C). Moreover, we performed coimmunoprecipitations and found that endogenous aPKC associated with endogenous Mst1/2 in both MDCK and NMuMG cell lysates (Supplemental Figure S6, C and D). Of interest, the interaction between aPKC and Mst1/2 was not dependent on cell density. This indicates that aPKC forms a complex with Mst1/2 and Sav1 but not Lats1/2. Although we did not detect an interaction between aPKC and Lats, we examined whether aPKCζ-ca expression affected Lats1/2 localization. Our Lats antibody did not work for immunostaining in MDCK cells; however, in NMuMG cells, Lats1 was localized to cell borders and colocalized with ZO-1 in both GFP control and aPKCζ-ca cells, indicating that aPKCζ-ca expression does not regulate Lats localization in 2D epithelial cultures (Supplemental Figure S6F). In control 3D structures, weak Lats staining was observed at the apical membrane but was diffuse in aPKCζ-ca structures, which do not form lumen (Supplemental Figure S6G). Disrupted localization of Lats1/2 in 3D is likely a secondary consequence of disrupted apical-basal polarity. Therefore, aPKCζ-ca associates with and affects the localization of the Mst/Sav1 complex.

If aPKC disrupts membrane localization of Mst1/2 to deregulate Yap1 localization and cell growth, then we hypothesized that restoring Mst1/2 to the plasma membrane in aPKCζ-ca cells would restore normal Yap1 localization and block epithelial overgrowth. To test this possibility, we expressed wild-type and myristoylated-Mst1 (myr-Mst) in control or aPKCζ-ca MDCK cells. We observed that wild-type Mst was predominantly cytoplasmic and did not rescue aPKCζ-ca phenotypes; however, myristoylated Mst was able to both exclude Yap1 from the nucleus and block epithelial overgrowth in 3D cultures (Figure 5, E–H, and Supplemental Figure S6H). Therefore these data support a model by which aPKC regulates Hippo signaling and epithelial growth by controlling Mst/Sav1 localization at the membrane.

Loss of Amot is necessary for cell shape and growth defects induced by aPKC gain of function in MDCK cells

To further understand potential changes to the Hippo pathway caused by aPKCζ-ca, we examined the protein expression of additional pathway members. Of interest, in addition to reduced Lats1/2 Ser909 phosphorylation, we observed a robust down-regulation of Amot, whereas Rassf1A, another Mst1/2-interacting protein, was unaltered (Supplemental Figure S7A). The expression of another tight junction protein, ZO-1, was also unaffected, demonstrating that the effect is specific to Amot, consistent with our earlier results showing that ZO-1 is retained at cell junctions. It was reported that Amot expression is regulated by protein stability and that phosphorylation by Lats1/2 prevents Amot degradation. Because pLats1/2 is reduced by aPKCζ-ca, we asked whether the observed loss of Amot was due to proteosome-dependent degradation. We treated cells with the proteosome inhibitor MG132 and observed that cells treated with the inhibitor were able to maintain Amot expression, indicating that Amot protein stability is affected (Supplemental Figure S7B).

Knockdown of Amot produces phenotypes that resemble our observed aPKCζ gain-of-function phenotypes in MDCK cells, including spindly shaped cells and deregulation of Yap1 localization (Zhao *et al.*, 2011). Therefore we hypothesized that loss of Amot expression may be a crucial event in the transformed phenotype induced by aPKCζ gain of function. To examine this possibility, we expressed Amot in control and aPKCζ-ca cells; as a control, we alternatively expressed AmotΔN, which does not localize to tight junctions and is not implicated in regulating the actin cytoskeleton or Yap1 signaling (Moleirinho *et al.*, 2014; Supplemental Figure S7, C–E). In 2D cultures, expression of Amot, but not AmotΔN, was able to restore Yap1 exclusion from the nucleus (Figure 6, A and B, and Supplemental Figure S7, F and G). On closer examination, we also observed that Yap1 localized to cell–cell junctions in control MDCK cells, as previously reported (Zhao *et al.*, 2011), but this localization was lost in aPKCζ-ca cells (Figure 6C). Of importance, expression of Amot, but not AmotΔN, was able to restore Yap1 localization to cell junctions (Figure 6C), consistent with a role for Amot in sequestration of Yap1 at tight junctions in MDCK cells (Zhao *et al.*, 2011). Furthermore, we found that expression of Amot, but not AmotΔN, rescued aPKCζ-ca cells from stratified growth in 2D cultures, which is consistent with this phenotype being driven by Yap1 activity and Amot sequestering Yap1 from the nucleus (Figure 6, D and E). Finally, Amot expression, but not AmotΔN, also rescued the spindly phenotype to restore a cobblestone appearance of aPKCζ-ca–expressing cells (Figure 6, F and G, and Supplemental Figure S7, H and I). In NMuMG cells, despite aPKCζ-ca also reducing phosphorylated Lats1/2 and affecting Yap1 localization, Amot expression was not altered by aPKCζ-ca expression (Supplemental Figure S3C). Furthermore, cell shape was not altered and Yap1 was not detected at cell membranes in NMuMG cells (Supplemental Figures S1, F and G, and 3C), indicating that the mechanism through which the Hippo pathway regulates Amot and Yap1 is context dependent.

Amot acts as a scaffold and can bind multiple components of the Hippo pathway, including Mst1/2, Lats1/2, and Yap1 (Moleirinho *et al.*, 2014). It is therefore possible that loss of Mst1/2 from cell–cell

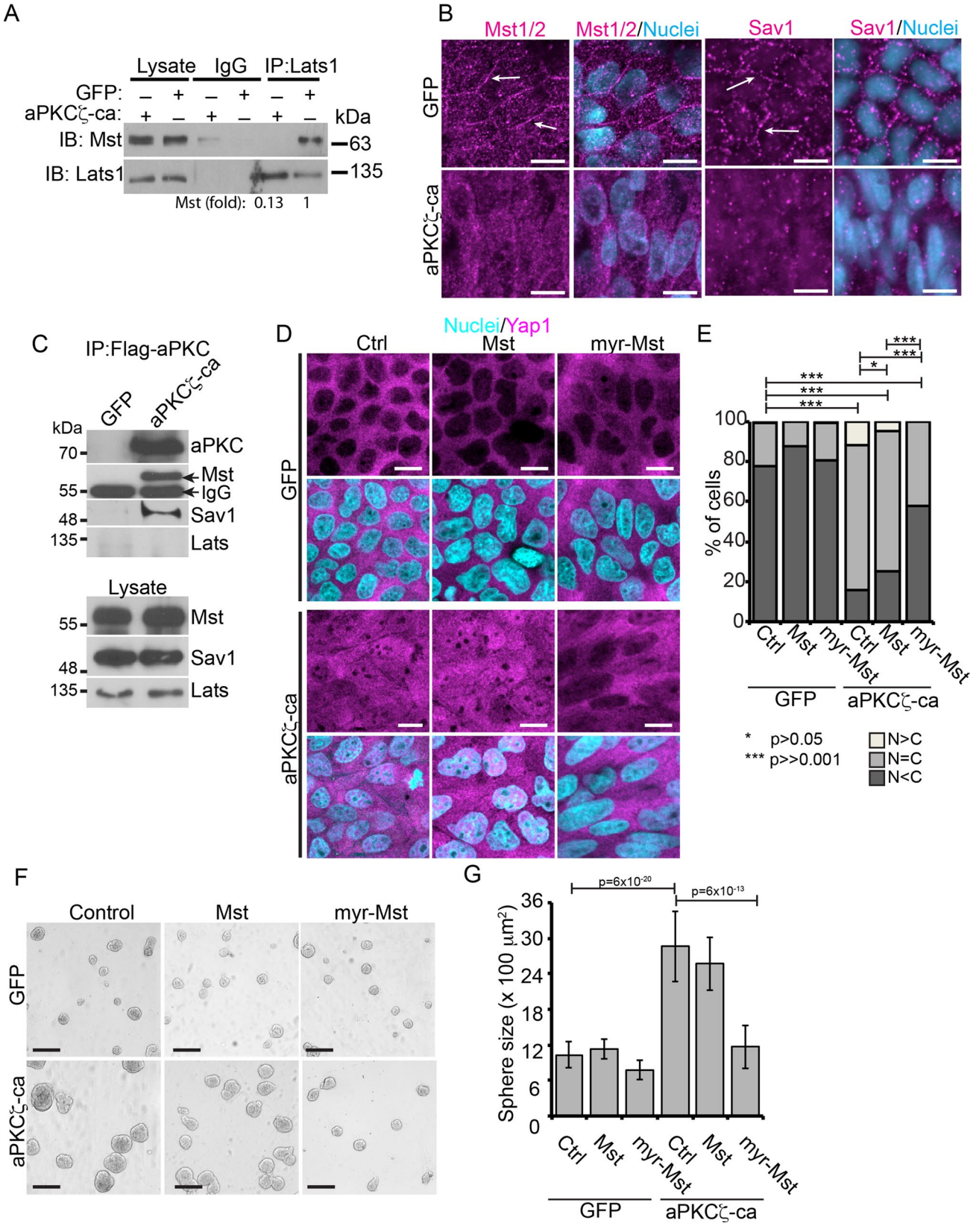

FIGURE 5: aPKC disrupts the Hippo complex. (A) Immunoblot showing the interaction between endogenous Mst1/2 and Lats1/2. Lats1 was immunoprecipitated from GFP- (control) and aPKCζ-ca–expressing MDCK cell lysates and immunoblotted for Mst1/2 and Lats1. Mst1/2 was quantified from $N = 3$ blots and normalized to the amount of Lats pulled down. (B) Immunofluorescence images showing confluent GFP and aPKCζ-ca cells immunostained for Mst1/2 or Sav1. Arrows show examples of localization at cell borders. (C) Immunoblot showing an interaction between Flag-tagged aPKCζ-ca and endogenous Mst1/2 and Sav1. Blot is representative of three independent experiments. (D) Images

junctions and reduced phosphorylation of Lats1/2 are due to loss of Amot expression. If this were the case, we expect that reexpression of Amot would restore Mst1/2 to the membrane and Lats1/2 phosphorylation. However, we did not observe relocalization of Mst1/2 to the plasma membrane or phosphorylation of Lats1/2 and Yap1 in aPKCζ-ca cells when Amot expression was restored (Figure 7, A and B), indicating that disruption of Mst1/2 localization and Lats1/2 phosphorylation is upstream of Amot rather than a consequence of loss of Amot expression in these cells.

We next evaluated whether Amot was required for transformed phenotypes associated with aPKC gain of function in MDCK 3D cultures. Reexpression of Amot reduced growth of aPKCζ-ca structures but did not restore lumen formation or polarity (Figure 7, C–E, and Supplemental Video S7). In contrast, AmotΔN expression did not rescue any of the aPKCζ-ca phenotypes but instead caused overgrowth that was not associated with translocation of Yap1 to the nucleus and formed 3D structures with multiple lumen (Figure 7E and Supplemental Figures S7, F–I, and S8, A and B), consistent with reports that AmotΔN promotes cell proliferation (Levchenko *et al.*, 2004). We confirmed that Amot expression does not affect aPKCζ-ca expression, ruling out the possibility that the rescued phenotype was due to down-regulation of aPKCζ-ca (Supplemental Figure S8C). Finally, expression of Amot did not rescue overgrowth in aPKCζ-ca NMuMG cells, supporting that Amot is not involved in overgrowth by aPKCζ-ca in NMuMG cells (Supplemental Figure S7, D and E).

Increased aPKC activity correlates with increased nuclear localization of Yap1 in human cancers

Our results indicate that aPKC expression is sufficient for loss of growth control in epithelial cells. To examine the relevance of this in human cancers, we evaluated the expression profile of aPKC isoforms across various tumors derived from epithelial tissues using data from The Cancer Genome Atlas (TCGA; http://cancergenome.nih.gov). We observed that both the iota and zeta isoforms were up-regulated in most cancer types examined and were less frequently down-regulated in some patients (Supplemental Figure S9A). To validate further the significance of our results, we examined the correlation between aPKC expression and nuclear Yap1 for lung squamous cell carcinoma (SCC) and ovarian carcinoma, two cancer types with frequent up-regulation of aPKCs. First, we immunostained a tissue microarray of lung SCC that contained 150 cores. Cores that did not contain a significant epithelial compartment or were damaged were omitted from analysis, leaving 107 cores for analysis. We coimmunostained the tissue microarray (TMA) for aPKC and Yap1 and then imaged all cores using an automated confocal microscope. The average pixel intensity from five regions of each core was measured, and tumors were grouped into those with low, medium, or high PKC intensity (Figure 8A). We then scored the nuclear/cytoplasmic localization of Yap1 for each core. We observed a strong correlation (Pearson's $r = 0.8$) between aPKC intensity and the proportion of cells with nuclear-enriched Yap1 (Figure 8, B and C). Both aPKC expression and the proportion of cells with Yap1 enriched in the nucleus correlated with lung tumor grade and stage (Figure 8D).

We further examined a 24-core TMA from serous ovarian carcinoma, a second tumor type that frequently has up-regulation of aPKC, and performed a similar analysis to the lung TMA (Supplemental Figure S9B). Similar to lung cancer, we observed a strong correlation between aPKC intensity and the proportion of cells with nuclear enriched Yap1 (Pearson's $r = 0.74$), and cores with polarized aPKC rarely had Yap1 enriched in the nucleus (Supplemental Figure S9, C and D). Therefore tumors with high aPKC have nuclear enrichment of Yap1, which supports our findings that aPKC regulates Yap1 localization and epithelial proliferation, indicating that the effect of aPKC on disrupting the Hippo pathway may be clinically relevant.

DISCUSSION

The activity and expression of aPKC isoforms are elevated in many epithelial cancer types and are associated with higher tumor grade and size, invasion, and poor survival (Kojima *et al.*, 2008; Yao *et al.*, 2010; Paul *et al.*, 2014). Here we report that overexpression of wild-type or active aPKC is sufficient to induce overgrowth phenotypes that are characteristic of potent oncogenes with transforming properties, such as ErbB2, Ras, Src, and PI3K (Kadono *et al.*, 1998; Aranda *et al.*, 2006; Zhang *et al.*, 2008; Hogan *et al.*, 2009; Toyli *et al.*, 2010; Sakurai *et al.*, 2012; Linch *et al.*, 2014). We demonstrate that when expressed in polarized epithelial cells, aPKCζ-ca induces loss of apical-basal polarity, disrupted epithelial organization, and loss of epithelial contact-inhibited growth control. Previous loss-of-function studies showed that aPKC plays a role in proliferation and loss of polarity in the context of established tumor cells and downstream of oncogenes (Aranda *et al.*, 2006; Yao *et al.*, 2010; Linch *et al.*, 2014; Paul *et al.*, 2014). Our work extends this by indicating that aPKC may be a driver oncogene in some cancers. Although less frequently, aPKCζ was reported to be down-regulated in some cancers, which correlates with therapeutic resistance and tumor recurrence (Pu *et al.*, 2012; Namdarian *et al.*, 2013). This suggests that aPKCs may have both oncogenic and tumor-suppressive functions, which affect different aspects of cancer progression.

Loss of apical-basal polarity, luminal filling, and loss of contact inhibition are characteristics of a transformed phenotype in epithelial cancers, and we report that aPKC gain of function is sufficient for many of these features. This is distinct from loss-of-function phenotypes of aPKC and other polarity proteins in 3D culture systems, which instead cause multiluminal structures that nonetheless retain apical identity (Jaffe *et al.*, 2008; Hao *et al.*, 2010; Durgan *et al.*, 2011). This suggests that loss of individual apical polarity proteins may be insufficient for loss of membrane polarity and luminal filling during epithelial transformation. Of interest, we found that aPKCζ-ca was mislocalized from the plasma membrane and induced the nonpolarized distribution of apical-basal polarity markers. This finding is consistent with observations that aPKC is mislocalized in more aggressive cancers (Kojima *et al.*, 2008; Du *et al.*, 2009). Furthermore, our results are consistent with observations in *Drosophila*, in which expression of membrane-targeted DaPKC induced nonpolarized localization of apical proteins (Sotillos *et al.*, 2004), and suggest that elevated aPKC expression or activity may be an important driver of polarity loss and early transformation events. Indeed, blocking aPKC is able to block transformation by various oncogenes, and

showing Yap1 localization in GFP or aPKCζ-ca cells with or without expression of Mst or myristoylated Mst (myr-Mst). (E) Quantification of the nuclear/cytoplasmic localization of Yap1 shown in D. Three independent fields/duplicate experiment. (F) Phase contrast images showing GFP- and aPKCζ-ca–expressing cells with Mst or myr-Mst grown in 3D culture. (G) Quantification of the size of 3D structures from cultures shown in F. We measured 130 GFP, 204 GFP/Mst, 120 GFP/myr-Mst, 103 aPKCζ-ca, 113 aPKCζ-ca/Mst, and 81 aPKCζ-ca/myr-Mst structures. Bars, 10 μm.

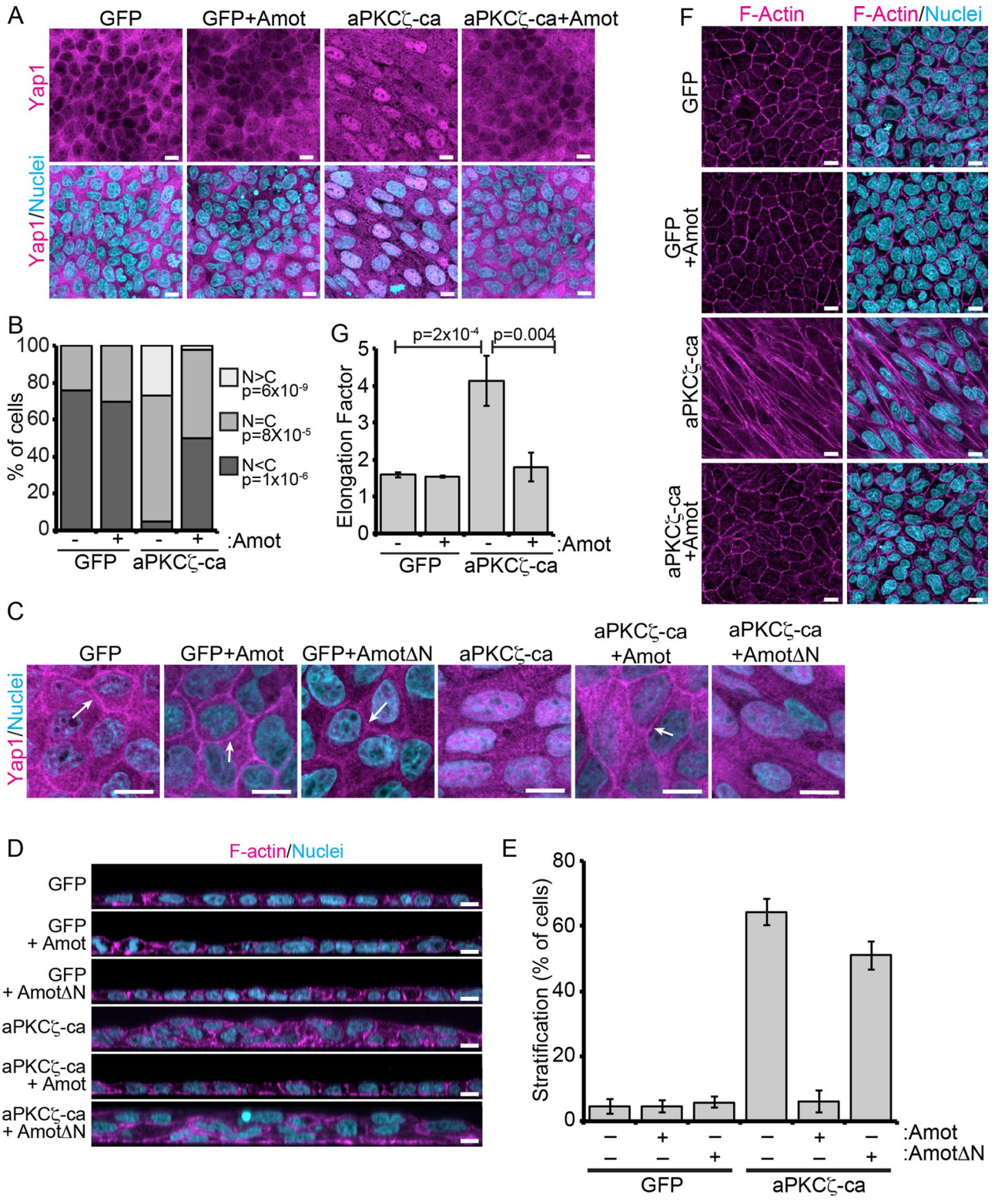

FIGURE 6: Amot rescues aPKCζ-ca–induced cell organization and growth defects. (A) Immunofluorescence images showing confluent GFP and aPKCζ-ca MDCK cells with or without Amot and immunostained for Yap1. (B) Quantification of the nuclear/cytoplasmic localization of Yap1. Three independent fields/duplicate experiment. (C) Fluorescence images showing Yap1 localization (arrows indicate staining at cell junctions). (D) Fluorescence *xz*-projections of GFP (control) and aPKCζ-ca cells coexpressing Amot or AmotΔN stained with phalloidin to visualize F-actin. (E) Quantification of cell stratification. More than five fields/duplicate experiment. (F) Fluorescence images showing cells stained with phalloidin to label F-actin. (G) Quantification of cell elongation factor (long axis/short axis). Three independent fields/triplicate experiment. Bars, 10 μm. Error bars, SD. The *p* values were calculated using one-way ANOVA and Tukey HSD post hoc tests.

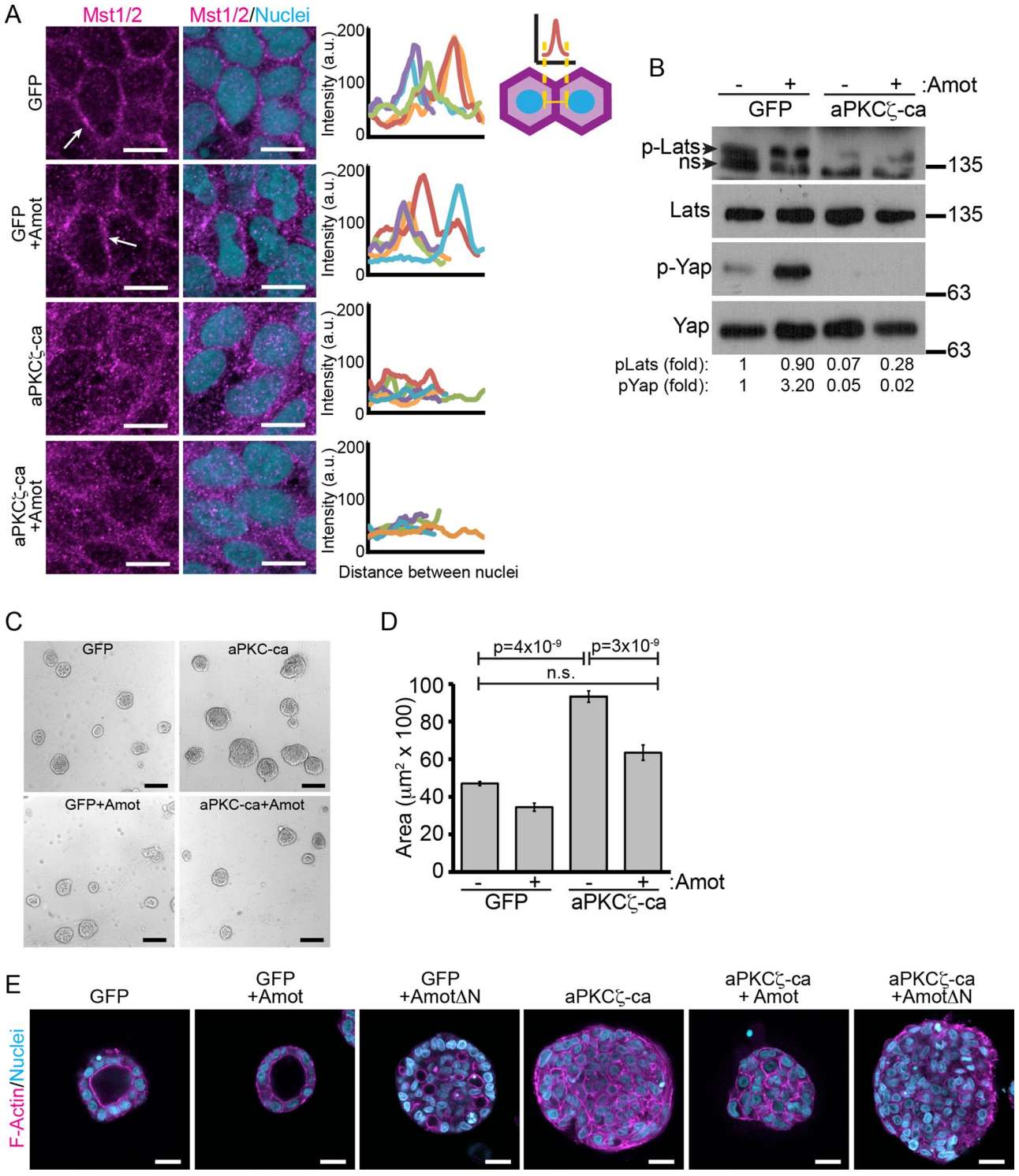

FIGURE 7: Amot rescues defects in epithelial organization and growth caused by aPKC gain of function in MDCK cells. (A) Immunofluorescence images showing Mst1/2 localization. Arrows show Mst1/2 at cell borders. Right, intensity of Mst1/2 across cell boundaries. Enrichment at the cell border is seen as a tall spike in intensity. Tracings from six cells. (B) Immunoblot showing expression of phospho-S909 Lats1/2 and phospho-Ser127 Yap1 in GFP (control) and aPKCζ-ca cells with or without Amot. ns, nonspecific band. Fold changes were determined from two blots. (C) Phase contrast images of 3D structures from GFP- (control) and aPKCζ-ca–expressing cells coexpressing Amot. (D) Quantification of the size of individual structures. We measured 516 GFP, 288 GFP+Amot, 281 aPKCζ-ca, and 173 aPKCζ-ca +Amot structures. (E) Fluorescence images of control or aPKCζ-ca 3D structures coexpressing Amot or AmotΔN and stained with phalloidin to visualize F-actin. Bars, 10 μm (A, E), 100 μm (C). Error bars, SD. The *p* values were calculated using one-way ANOVA and Tukey HSD post hoc tests.

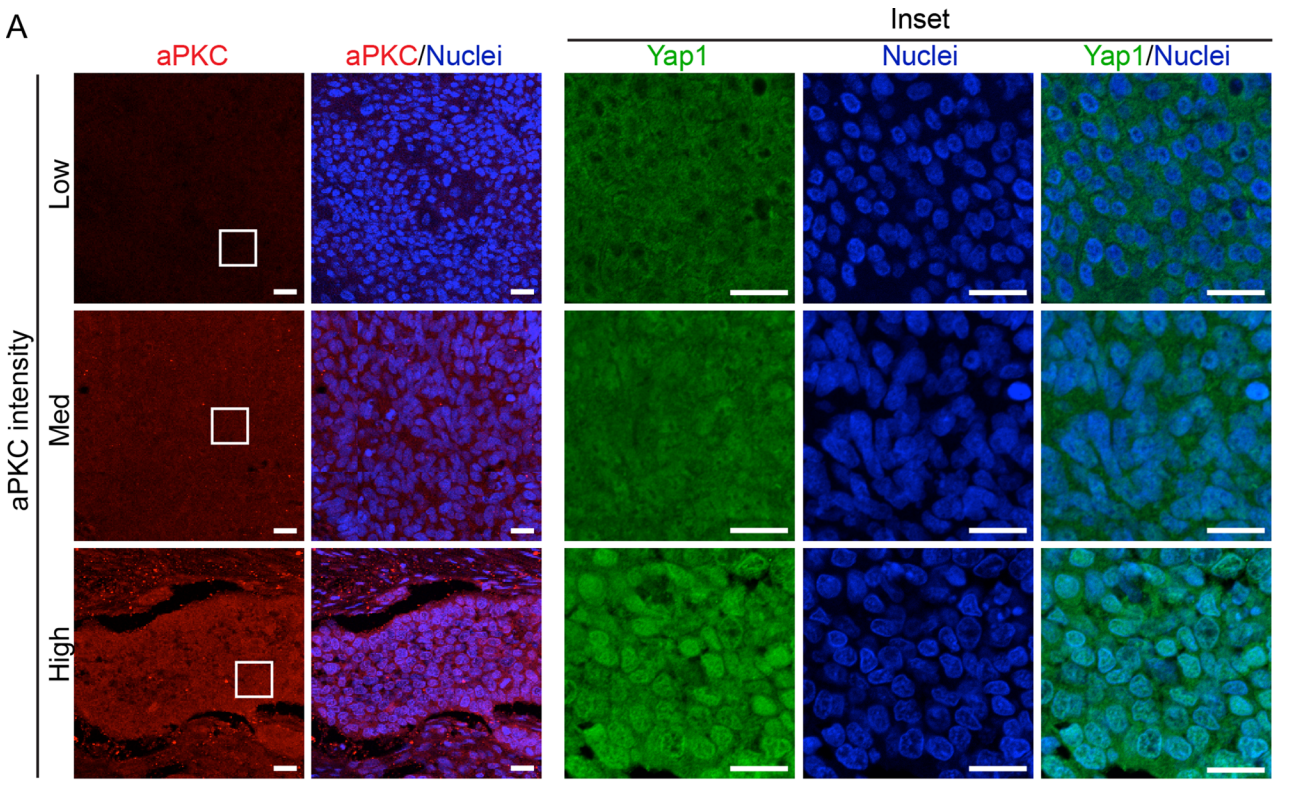

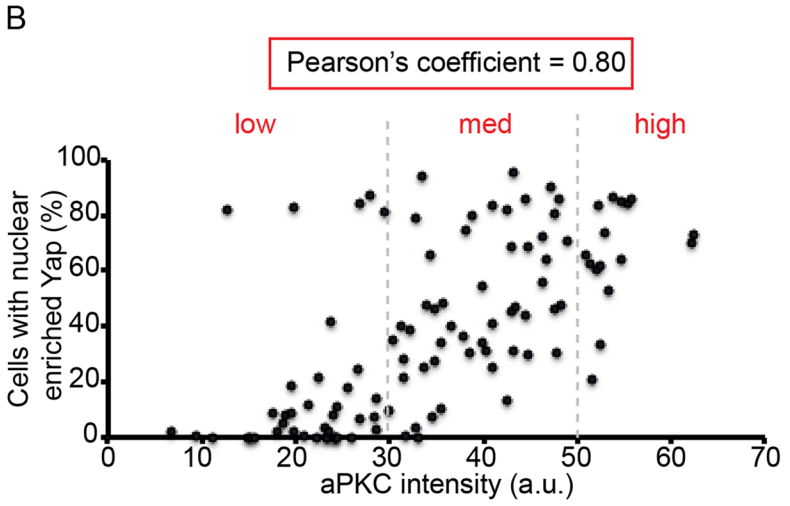

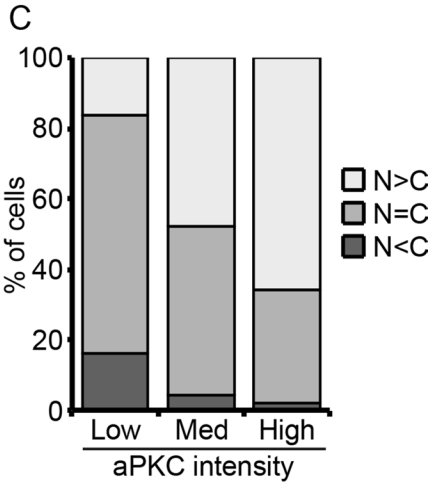

D

		Grade	Stage
aPKC intensity	Spearman's coeff	0.219	0.188
	p-value	0.027	0.021
% Nuclear Yap1	Spearman's coeff	0.56	0.425
	p-value	7.8E-14	6.0E-8

FIGURE 8: aPKC expression correlates with nuclear Yap1 in human lung cancers. (A) Representative images showing low, medium, and high aPKC intensity and Yap1 localization from a TMA containing lung squamous carcinoma samples. Bars, 25 μm. (B) Scatter plot showing aPKC intensity and percentage of cells with Yap1 enriched in the nucleus. aPKC intensity was binned into low, medium, and high (vertical gray dotted lines). (C) Quantification of the nuclear/cytoplasmic localization of Yap1 in samples with low, medium, or high aPKC intensity. (D) Spearman's coefficients and associated *p* values for aPKC expression and Yap1 nuclear localization with lung cancer grade and stage.

cells retain apical-basal polarity (Aranda *et al.*, 2006; Linch *et al.*, 2014). Because lumen formation is a stepwise process from which a preapical patch expands to a differentiated apical membrane surrounding a central lumen (Ferrari *et al.*, 2008; Bryant *et al.*, 2010), the inability of aPKCζ-ca cells to specify an apical domain or form microlumen underlies the failure to establish a luminal cavity and indicates a role for aPKC in the earliest stages of polarization.

An important observation is that aPKC overexpression is able to overcome contact-inhibited growth. Contact-inhibited growth of epithelial cells is perhaps best understood in MDCK monolayers and is dependent on mechanical constraints of cell density (Puliafito *et al.*, 2012). We report that in 2D cultures, aPKCζ-ca induces cells to grow as stratified foci, consistent with loss of contact-inhibited growth (Eisenhoffer and Rosenblatt, 2013). Hippo/Yap1 signaling is an established pathway to control contact-inhibited growth of epithelial cells. The stratified phenotype induced by aPKC-ca expression in 2D cultures is reminiscent of Yap1 overexpression (Zhao *et al.*, 2011). We observed that aPKC gain of function induces nuclear accumulation of Yap1 and that aPKC-induced 2D multilayering was dependent on Yap1 function. In 2D cultures, epithelial contact inhibition occurs through distinct steps starting with reduced cell motility, followed by rapid polarization, and finally reduced proliferation, which couples with cell elimination to maintain epithelial homeostasis (Puliafito *et al.*, 2012; Eisenhoffer and Rosenblatt, 2013). Whether contact inhibition occurs through similar stages in 3D systems is not known. However, our data support a model in which mechanical constraints, rather than cell–cell interfaces, also regulate contact-inhibited growth in 3D environments, since normal polarized structures reach a maximal size and then maintain this size (Supplemental Figure S1A). However, the role of polarity in this may differ between 2D and 3D environments, since the establishment of cell polarity is an early event in 3D cultures, occurring soon after two cells form an adhesion interface (Bryant *et al.*, 2010). Moreover, aPKC gain of function and Yap1 overexpression are both able to increase the size of 3D structures to a similar degree, with the former comprising a solid mass of nonpolarized cells and the latter retaining apical-basal polarity. Nonetheless, the solid structures would contain more cells than polarized structures of equal size, and loss of polarity may allow for tighter packing of cells and a stronger loss of contact inhibition. Although aPKC gain of function increases the proliferation rate to increase cell numbers, the phenotype is true loss of contact-inhibited growth because structures continue to grow beyond the size limit of normal control structures.

It is established in both *Drosophila* and mammalian models that cell-adhesion and cell-polarity proteins are crucial regulators of signaling through the Hippo pathway to affect Yap/Taz function in contact-inhibited growth (Genevet and Tapon, 2011; Varelas and Wrana, 2012). An emerging view is that different adhesion and polarity regulators control Hippo signaling through distinct mechanisms. For example, in *Drosophila*, Lgl, Crb3, and Scrib can control scaffolding and localization of various Hippo pathway components to control Yki (Yap/Taz) activity (Grzeschik *et al.*, 2010; Yang *et al.*, 2015). Depletion of basolateral Lgl in the developing *Drosophila* eye disk acts through aPKC to mislocalize Hpo and its negative regulator RASSF1, whereas Crb3 regulates Expanded localization (Grzeschik *et al.*, 2010). Moreover, basolateral Scrib and adherens junctions regulate scaffolding of Hippo components and regulate Yki activity through cell-autonomous and non–cell-autonomous mechanisms, respectively (Yang *et al.*, 2015). Of interest, loss of Scrib or adherens junction proteins (E-cad and α-cat) results in mislocalization of aPKC from the apical membrane, but the contribution of aPKC in this context is not known (Yang *et al.*, 2015). Our data extend these to mammalian systems and further demonstrate that aPKC can associate with the Mst/Sav1 complex to regulate its apical localization and coupling with Lats1/2. The presence of multiple inputs into regulating Yap/Taz function likely enables cells to fine-tune proliferation control based on cell density. As such, more severe disruption of epithelial integrity would release multiple Yap/Taz pools to promote a strong proliferative response. Aragona *et al.* (2013) proposed a two-step model for contact-inhibited proliferation in which cell adhesion accounts for some regulation of Yap/Taz, whereas cell and tissue mechanics provide a backup mechanism by regulating the actin cytoskeleton to regulate contact-inhibited proliferation (Piccolo *et al.*, 2014).

Of interest, although Yap1 overexpression generated enlarged 3D structures, they retained apical-basal polarity and formed multiple lumens. Because a multilumen phenotype is frequently observed when individual polarity proteins are depleted, this may indicate that Yap1 affects the polarity machinery. However, increased proliferation may also promote a multilumen phenotype (Cerruti *et al.*, 2013), which may alternatively explain the effect caused by Yap1. Nonetheless, Yap1 overexpression is not sufficient for loss of apical-basal polarity and luminal filling, and therefore aPKC gain of function produced a stronger phenotype than Yap1 alone. Of interest, Yap1 overexpression in the mammary gland is not sufficient to induce hyperplasia or tumorigenesis (Chen *et al.*, 2014). The relatively weak transforming potential of Yap1 may reflect the fact that in MDCK cells and the mammary gland, overexpressed Yap1 is not restricted to the nucleus (Chen *et al.*, 2014), indicating that normal polarized cells have robust mechanisms to exclude Yap from the nucleus and suppress overgrowth. Of importance, Yap1 is required for tumor growth downstream of the polyoma middle T antigen under the mammary-specific MMTV promoter (Chen *et al.*, 2014), and we observed that it is necessary downstream of aPKC for overgrowth phenotypes, indicating that other processes, possibly loss of polarity, establish a permissive state for Yap1 to enter the nucleus and promote transformed growth.

We report that aPKC expression was associated with loss of Amot in MDCK cells, which is able to recruit Yap1 to cell junctions (Zhao *et al.*, 2011). Indeed, we found that Yap1 was not localized to cell junctions in aPKC gain of function cells but was restored by reexpressing Amot, which also blocked aPKC-induced overgrowth. This indicates that Amot is an important link between aPKC and Yap1 in controlling proliferation in some cells. How might aPKC regulate Amot stability? Lats1/2 was reported to phosphorylate and stabilize Amot by protecting it from degradation (Chan *et al.*, 2013). Our data show that Lats1/2 activity is diminished and that inhibiting the proteosome maintains Amot levels, supporting this model. Previously aPKC was implicated in Hippo signaling in *Drosophila*, but whether a similar link occurred in mammals was not known (Grzeschik *et al.*, 2010). Our results provide strong evidence that aPKC can affect Yap1 localization by acting through Amot. Because an Amot orthologue has not been identified in flies, this indicates that the mechanism identified here may be unique to mammals. Of interest, we did not observe loss of Amot from NMuMG cells, and aPKCζ-ca was not associated with cell shape changes in this cell model. Furthermore, overexpression of Amot did not block overgrowth by aPKCζ-ca in these cells. Therefore this suggests that among mammalian epithelia, the mechanisms that regulate Yap1 localization can differ. The basis for this difference is not known, but it may reflect differences in the expression of Amot family members, which can vary among cell lines and may exist in different protein complexes (Moleirinho *et al.*, 2014).

In addition to disrupted cell polarity and growth dynamics, we found that aPKC gain of function induced a dramatic change in cellular morphology from a cobblestone appearance to an elongated, spindle-like morphology in MDCK cells. Remarkably, cell shape was completely reversed by reexpression of Amot, indicating that Amot regulates both cell shape changes and Yap1 localization in aPKC-ca cells. Although reexpression of Amot was sufficient to restore Yap1 at tight junctions, it did not restore the plasma membrane localization of Mst1/2 or Lats1/2 phosphorylation, indicating that loss of Mst1/2 from the plasma membrane and inactivation of Lats1/2 are upstream of loss of Amot expression. Of interest, despite restoring Yap1 to junctions, Amot reexpression did not restore phosphorylation of Yap1 on Ser-127. This site is phosphorylated by Lats1/2 and is consistent with Lats1/2 remaining inactive. This also suggests that phosphorylation of Yap1 is unlikely to be required for association with Amot at tight junctions, unlike adherens junctions, where 14-3-3 links phosphorylated Yap1 to α-catenin (Schlegelmilch *et al.*, 2011).

We propose the following model for how aPKC may overcome contacted-inhibited growth by deregulating the Hippo/Yap1 pathway. Mst1/2 associates with aPKC, and due to loss of apical-basal polarity and aPKC delocalization, Mst1/2 becomes mislocalized from the plasmas membrane. This prevents Lats1/2 activation by Mst1/2, and reduced Lats1/2 activity fails to phosphorylate and protect Amot from degradation (in MDCK cells). Loss of Amot has two major effects: it deregulates the actin cytoskeleton, causing cytoskeletal and cell shape changes, and, in parallel, it prevents Yap1 from being sequestered at junctions, resulting in nuclear accumulation of Yap1 and increased proliferation (Figure 9, A and B). An alternative mechanism occurs in NMuMG cells, by which Yap1 nuclear translocation and overgrowth are independent of loss of Amot, indicating that different epithelial cells may differentially wire Hippo/Yap1 signaling.

Hippo signaling and aPKC are both frequently disrupted in human cancers. Of importance, we identified a strong correlation between aPKC expression and Yap1 nuclear localization in both lung squamous cell carcinoma and ovarian serous adenocarcinoma, two tumor types with high aPKC expression. This supports the possible clinical relevance of our findings and that aPKC expression may help drive tumorigenesis in these tissues by disrupting contact-inhibited growth through Hippo signaling.

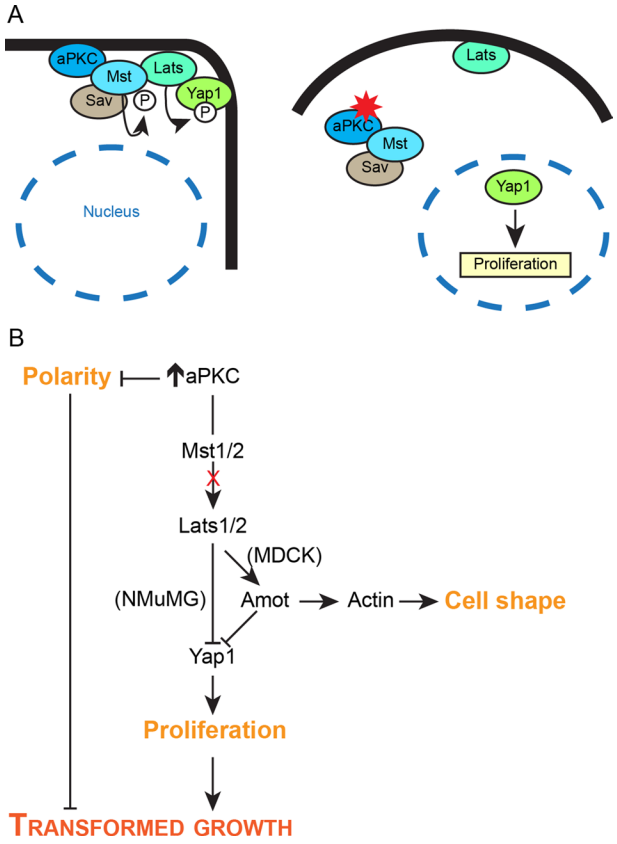

FIGURE 9: Summary and model for aPKC gain of function in epithelial cell transformation. (A) Proposed model of how aPKC deregulates Hippo signaling. aPKC binds Mst1/2, which delocalizes it from cell junctions. Mislocalized Mst1/2 uncouples from Lats1/2 and prevents its phosphorylation and activity, freeing Yap1 to enter the nucleus to promote proliferation. (B) Proposed pathways by which aPKC gain of function induces a transformed epithelial phenotype.

MATERIALS AND METHODS

Cell culture

MDCK, 293LT, and NMuMG cells were grown in DMEM (Wisent) supplemented with 10% fetal bovine serum (Wisent, Saint-Jean-Baptiste, Canada), penicillin/streptomycin (Sigma-Aldrich, Oakville, Canada), and 10 μg/ml insulin (NMuMG only). For 3D cultures, single-cell suspensions were plated on a thin layer of 100% Geltrex (Invitrogen) on cover glasses in media supplemented with 2% Geltrex. To inhibit the proteosome, cells were treated for 4 h with 10 μM (final concentration) MG132 (Sigma-Aldrich).

Plasmids, lentivirus production, and cell infection

Lentivirus was produced in 293LT cells by cotransfecting 50 μg of pWPI lenti-plasmid (Addgene plasmid 12254) with 37.5 μg of psPAX2 packaging plasmid (Addgene plasmid 12260) and 15 μg of envelope plasmid pMD2.G (Addgene plasmid 12259; all from D. Trono, Ecole Polytechnique Federale de Lausanne, Switzerland), using calcium phosphate precipitation in 15-cm dishes. Viral supernatant was collected 48 h after transfection and precipitated overnight in 10% PEG-8000. The resulting precipitate was collected by centrifugation at 4000 × *g* for 30 min, and the pellet was resuspended in 300 μl of cell culture medium and stored at –80°C. Concentrated virus was tittered using 293LT cells. MDCK cells were infected with lentivirus at a multiplicity of infection of 20 using spinfection at 300 × *g* for 3 h. In all cases, cells were sorted for GFP-fluorescence by fluorescence-activated cell sorting at the McGill University Flow Cytometry Core Facility. The same instrument settings and gates were used for each cell line, and GFP fluorescence was checked regularly and cells replenished if population drift occurred.

Lenti-GFP-Amot (Addgene plasmid 32828) and Lenti-GFP-AmotΔN (Addgene plasmid 32830) were generated by K. Guan (University of California, San Diego, La Jolla, CA). pJ3H-Mst1 was a gift from Jonathan Chernoff (Fox Chase Cancer Center, Philadelphia, PA; Addgene plasmid 12203). Mst1 was cloned into the pWPI vector and produced as lentivirus. For myristoylated Mst1, the c-src myristoylation signal sequence was added to the N-terminus of Mst1 and was generated as a gBlock (IDT, Coralville, IA) and then ligated into pWPI.

Antibodies

Primary antibodies and concentrations used were as follows: rabbit anti–aPKC-C20 (1:100, immunofluorescence [IF], or 1:1000, immunoblotting [IB]; sc-216, Santa Cruz Biotechnology, Dallas, TX), rabbit anti-FLAG (1:1000; DB125, Delta Biolabs, Gilroy, CA), mouse anti–α-tubulin (1:10,000; T9026, Sigma-Aldrich), mouse anti-Yap1 (1:100 [IF] or 1:1000 [IB]; 63.7, sc-101199, Santa Cruz

Biotechnology), rabbit anti-Yap1 (1:100; H-125, sc-15407, Santa Cruz Biotechnology), rabbit anti–phospho Ser127-Yap1 (1:1000; 4911S, Cell Signaling Technology, Beverly, MA), rabbit anti-Mst1/2 (1:100 [IF] or 1:1000 [IB]; A300-477A, Bethyl Labs, Montgomery, TX), rabbit anti-Mst (1:100; 3682S, Cell Signaling Technology), rabbit anti–phospho Thr180/182-Mst1/2 (1:1000; 9157S, Cell Signaling Technology), rabbit anti-Lats1/2 (1:1000; sc-12494, Santa Cruz Biotechnology), rabbit anti-Lats1/2 (1:1000; A300-477A; Bethyl Labs), rabbit anti–phospho-Ser909-Lats1/2 (1:1000 [IB]; 9157S, Cell Signaling Technology), mouse anti–Myc tag (1:1000 [IB]; 9E10-C, Developmental Studies Hybridoma Bank, University of Iowa, Iowa City, IA), mouse anti-Sav1 (1:500; 3057S, Cell Signaling Technology), mouse anti-Par6B (1:250; sc67392, Santa Cruz Biotechnology), rabbit anti-RASSF1A (1:1000; PA5-21322, Thermo Fisher Scientific, Burlington, Canada), mouse anti-actin (1:1000 [IB], sc-8432, Santa Cruz Biotechnology), rabbit anti-Ki67 (1:100 [IF]; ab15580, Abcam, Toronto, Canada), rabbit anti–cleaved caspase-3 (1:100 [IF]; 9661S, Cell Signaling Technology), mouse anti–E-cadherin (1:600 [IF] or 1:5000 [IB]; 610181, BD Biosciences, San Jose, CA), rabbit anti-Numb (ab14140; Abcam), and rat anti–ZO-1 (1:100 [IF] or 1:1000 [IB]; R26.4C-z, Developmental Studies Hybridoma Bank). F-Actin was labeled with Alexa Fluor 555–phalloidin (1:100; A34055, Invitrogen, Burlington, Canada).

Immunoblotting and immunoprecipitation

For immunoblotting, cells were washed twice with ice-cold phosphate-buffered saline (PBS) and then lysed in RIPA buffer (1 mM EDTA, 0.5 mM ethylene glycol tetraacetic acid, 150 mM NaCl, 1% Triton X-100, 0.1% sodium deoxycholate, 0.1% SDS, 10 mM Tris-HCl, pH 8.0) containing a protease inhibitor cocktail (Roche, Laval, Canada). Equal amounts of protein were separated by SDS–PAGE on 8–12% gels and transferred to nitrocellulose membranes. Membranes were blocked in 5% dried milk powder in Tris-buffered saline/Tween 20 (TBST). Primary antibodies were diluted in TBST and incubated for 1 h at room temperature or overnight at 4°C. Membranes were washed three times with TBST and incubated for 1 h in horseradish peroxidase–conjugated secondary antibodies (Jackson ImmunoResearch, West Grove, PA) diluted 1:5000 in 3% milk powder/TBST for 1 h at room temperature. Bands were visualized using SuperSignal West Pico Chemiluminescent Substrate (Thermo Scientific) and exposure to UltraCruz radiographic film (Santa Cruz Biotechnology).

For immunoprecipitation, cells were washed twice with ice-cold PBS and then lysed in NP40 buffer (150 mM NaCl, 1% NP-40, 50 mM Tris-HCl, pH 8.0) containing a protease inhibitor cocktail (Roche). Lysates were precleared with MagnaBeads (Thermo Fisher Scientific) and then incubated with 2 µg of antibody or isotype control overnight at 4°C. Antibodies were captured with MagnaBeads (Thermo Scientific) and washed three times with lysis buffer. For immunoprecipitation of Mst1/2 and Lats1/2, CHAPS buffer (2% 3-[(3-cholamidopropyl)dimethylammonio]-1-propanesulfonate, 10 mM NaF, 1 mM $NaVO_4$, 100 nM calyculin A) with protease inhibitor cocktail was used instead of NP-40 buffer.

Immunofluorescence and confocal microscopy

Cells were fixed in 4% paraformaldehyde or methanol (at –20°C) for 20 min, permeabilized in 0.5% Triton X-100/0.1% bovine serum albumin for 20 min, and then blocked in 5% normal goat serum for 1 h. Cells were incubated with primary antibodies overnight at 4°C and in secondary antibodies for 1 h. To stain nuclei, cells were incubated in 1 µg/ml Hoechst 33258 for 15 min. For Mst1/2 staining, cells were fixed with methanol for 20 min at –20°C, blocked in 1× Roche Blocking Buffer (RBB; Roche), and incubated with antibodies in 0.5× RBB overnight at 4°C. Cells were mounted in FluorMount (Dako, Burlington, Canada) and imaged on an LSM-700 (Zeiss, Toronto, Canada) using 20× (numerical aperture [NA] 0.8) or 40× oil immersion lenses (NA = 1.4).

For long-term time-lapse experiments, 3D MDCK cultures were incubated, and bright-field images were captured for up to 151 h using an IncuCyteZoom (Essen Biosciences, Ann Arbor, MI) with a 10× objective lens.

Analysis and statistics

For analysis of growth dynamics, grayscale time-lapse image series were assembled as a stack in ImageJ (National Institutes of Health, Bethesda, MD). To all images in the stack, the Minimum filter was applied, followed by thresholding using the Intermodes method. A region of interest was drawn around individual 3D structures, and the Analyze Particles function was used with the following parameters: size (pixels^2) = 75–∞; include holes = True. Three-dimensional structures were excluded from analysis if they touched the edge of the frame at any time during the series or if two or more structures touched or merged. Results are from quadruplicate image positions from each of three experiments. The growth of 22–44 3D structures was measured for each experimental replicate, resulting in a total of 124 control and 93 aPKC structures being analyzed over 151 h. Resulting curves were fitted to fourth-degree polynomial functions (R^2 = 0.997, control; R^2 = 0.999, aPKC-ca), and the growth rates were determined using MATLAB (R2013b; MathWorks, Natick, MA). The slope of the curve at $t_{1/2}$ was determined by solving the first derivative at $t_{1/2}$ for each curve using MATLAB and represents the growth rate. The average of the three experimental replicates was plotted in Excel, with error bars representing SE. Analysis of variance (ANOVA) was calculated using MATLAB, and Student's *t* tests were calculated using Excel.

Images were contrast enhanced in ImageJ, and contrast was applied uniformly across each image and equally between comparative images. Images were pseudocolored in ImageJ.

For analysis of TCGA data, the TCGA Provisional data sets were used in all cases. A *z*-score of 2.0 was used as a cutoff for up- or down-regulation.

Tumor microarrays

TMAs for lung squamous cell carcinoma (LC1505) and serous ovarian adenocarcinoma (OV241) were purchased from US BioMax (Rockville, MD). TMAs were deparaffinized through HistoClear II (twice) and a series of 100/95/70% ethanol for 2 min each. Antigen retrieval was performed using Tris/EDTA, pH 9.0, buffer in pressure cooker for 7 min. Tissues were blocked in 10% goat serum for 1 h and then processed for immunofluorescence staining as described.

Cores that did not contain a significant epithelial compartment or that were damaged were omitted from analysis, leaving 107 cores for analysis.

For analysis, images of each core were taken using an automated confocal microscope (LSM700; Zeiss) with identical settings used for all cores. To measure aPKC intensity, the average pixel intensity from five tumor-containing regions of each core was measured, and tumors were grouped into those with low, medium, or high PKC intensity. To correlate the nuclear/cytoplasmic localization of Yap1 for each core, we applied a threshold to images of the nuclear stain (Hoechst 33342) and Yap1 channels using ImageJ. If the Yap1 signal overlapped the nuclear signal, it was counted as nuclear. If the nuclear intensity was greater than the surrounding cytoplasmic staining, it was scored as nuclear enriched. Tests for normality of data

were performed using the Shapiro–Wilk test in SPSS software. Correlations for normal data were determined using Pearson's coefficients, and Spearman coefficients were determined for nonparametric data using SPSS.

ACKNOWLEDGMENTS

We thank D. Trono (Ecole Polytechnique Federal de Lausanne, Switzerland) and K. Guan (University of California, San Diego, La Jolla, CA) for plasmids. We thank Ken McDonald of the McGill University Flow Cytometry Core for assistance with cell sorting. L.M. is a Fonds Recherche du Quebec–Santé Research Scholar (Junior I). M.A.M. was supported by a Defi Canderel studentship. A.L.S. was supported by a McGill Integrated Cancer Research Training Program summer studentship. This work was supported by a Canadian Institutes of Health Research grant to L.M. (MOP-119482).

REFERENCES

Adler JJ, Johnson DE, Heller BL, Bringman LR, Ranahan WP, Conwell MD, Sun Y, Hudmon A, Wells CD (2013). Serum deprivation inhibits the transcriptional co-activator YAP and cell growth via phosphorylation of the 130-kDa isoform of Angiomotin by the LATS1/2 protein kinases. Proc Natl Acad Sci USA 110, 17368–17373.

Aragona M, Panciera T, Manfrin A, Giulitti S, Michielin F, Elvassore N, Dupont S, Piccolo S (2013). A mechanical checkpoint controls multicellular growth through YAP/TAZ regulation by actin-processing factors. Cell 154, 1047–1059.

Aranda V, Haire T, Nolan ME, Calarco JP, Rosenberg AZ, Fawcett JP, Pawson T, Muthuswamy SK (2006). Par6-aPKC uncouples ErbB2 induced disruption of polarized epithelial organization from proliferation control. Nat Cell Biol 8, 1235–1245.

Atwood SX, Li M, Lee A, Tang JY, Oro AE (2013). GLI activation by atypical protein kinase C iota/lambda regulates the growth of basal cell carcinomas. Nature 494, 484–488.

Avruch J, Zhou D, Fitamant J, Bardeesy N, Mou F, Barrufet LR (2012). Protein kinases of the Hippo pathway: regulation and substrates. Semin Cell Dev Biol 23, 770–784.

Bryant DM, Datta A, Rodriguez-Fraticelli AE, Peranen J, Martin-Belmonte F, Mostov KE (2010). A molecular network for de novo generation of the apical surface and lumen. Nat Cell Biol 12, 1035–1045.

Cao X, Pfaff SL, Gage FH (2008). YAP regulates neural progenitor cell number via the TEA domain transcription factor. Genes Dev 22, 3320–3334.

Cerruti B, Puliafito A, Shewan AM, Yu W, Combes AN, Little MH, Chianale F, Primo L, Serini G, Mostov KE, *et al.* (2013). Polarity, cell division, and out-of-equilibrium dynamics control the growth of epithelial structures. J Cell Biol 203, 359–372.

Chan EH, Nousiainen M, Chalamalasetty RB, Schafer A, Nigg EA, Sillje HH (2005). The Ste20-like kinase Mst2 activates the human large tumor suppressor kinase Lats1. Oncogene 24, 2076–2086.

Chan SW, Lim CJ, Guo F, Tan I, Leung T, Hong W (2013). Actin-binding and cell proliferation activities of angiomotin family members are regulated by Hippo pathway-mediated phosphorylation. J Biol Chem 288, 37296–37307.

Chen Q, Zhang N, Gray RS, Li H, Ewald AJ, Zahnow CA, Pan D (2014). A temporal requirement for Hippo signaling in mammary gland differentiation, growth, and tumorigenesis. Genes Dev 28, 432–437.

Chou MM, Hou W, Johnson J, Graham LK, Lee MH, Chen CS, Newton AC, Schaffhausen BS, Toker A (1998). Regulation of protein kinase C zeta by PI 3-kinase and PDK-1. Curr Biol 8, 1069–1077.

Cohen EE, Lingen MW, Zhu B, Zhu H, Straza MW, Pierce C, Martin LE, Rosner MR (2006). Protein kinase C zeta mediates epidermal growth factor-induced growth of head and neck tumor cells by regulating mitogen-activated protein kinase. Cancer Res 66, 6296–6303.

Cordenonsi M, Zanconato F, Azzolin L, Forcato M, Rosato A, Frasson C, Inui M, Montagner M, Parenti Anna R, Poletti A, *et al.* (2011). The Hippo transducer TAZ confers cancer stem cell-related traits on breast cancer cells. Cell 147, 759–772.

Desai S, Pillai P, Win-Piazza H, Acevedo-Duncan M (2011). PKC-iota promotes glioblastoma cell survival by phosphorylating and inhibiting BAD through a phosphatidylinositol 3-kinase pathway. Biochim Biophys Acta 1813, 1190–1197.

Dimri G, Band H, Band V (2005). Mammary epithelial cell transformation: insights from cell culture and mouse models. Breast Cancer Res 7, 171–179.

Du GS, Wang JM, Lu JX, Li Q, Ma CQ, Du JT, Zou SQ (2009). Expression of P-aPKC-iota, E-cadherin, and beta-catenin related to invasion and metastasis in hepatocellular carcinoma. Ann Surg Oncol 16, 1578–1586.

Durgan J, Kaji N, Jin D, Hall A (2011). Par6B and atypical PKC regulate mitotic spindle orientation during epithelial morphogenesis. J Biol Chem 286, 12461–12474.

Eder AM, Sui X, Rosen DG, Nolden LK, Cheng KW, Lahad JP, Kango-Singh M, Lu KH, Warneke CL, Atkinson EN, *et al.* (2005). Atypical PKCiota contributes to poor prognosis through loss of apical-basal polarity and cyclin E overexpression in ovarian cancer. Proc Natl Acad Sci USA 102, 12519–12524.

Eisenhoffer GT, Rosenblatt J (2013). Bringing balance by force: live cell extrusion controls epithelial cell numbers. Trends Cell Biol 23, 185–192.

Evans JD, Cornford PA, Dodson A, Neoptolemos JP, Foster CS (2003). Expression patterns of protein kinase C isoenzymes are characteristically modulated in chronic pancreatitis and pancreatic cancer. Am J Clin Pathol 119, 392–402.

Ferrari A, Veligodskiy A, Berge U, Lucas MS, Kroschewski R (2008). ROCK-mediated contractility, tight junctions and channels contribute to the conversion of a preapical patch into apical surface during isochoric lumen initiation. J Cell Sci 121, 3649–3663.

Fields AP, Frederick LA, Regala RP (2007). Targeting the oncogenic protein kinase Ciota signalling pathway for the treatment of cancer. Biochem Soc Trans 35, 996–1000.

Genevet A, Tapon N (2011). The Hippo pathway and apico-basal cell polarity. Biochem J 436, 213–224.

Glantschnig H, Rodan GA, Reszka AA (2002). Mapping of MST1 kinase sites of phosphorylation. Activation and autophosphorylation. J Biol Chem 277, 42987–42996.

Graybill C, Wee B, Atwood SX, Prehoda KE (2012). Partitioning-defective protein 6 (Par-6) activates atypical protein kinase C (aPKC) by pseudosubstrate displacement. J Biol Chem 287, 21003–21011.

Grifoni D, Garoia F, Bellosta P, Parisi F, De Biase D, Collina G, Strand D, Cavicchi S, Pession A (2007). aPKCzeta cortical loading is associated with Lgl cytoplasmic release and tumor growth in Drosophila and human epithelia. Oncogene 26, 5960–5965.

Grzeschik NA, Parsons LM, Allott ML, Harvey KF, Richardson HE (2010). Lgl, aPKC, and Crumbs regulate the Salvador/Warts/Hippo pathway through two distinct mechanisms. Curr Biol 20, 573–581.

Halaoui R, McCaffrey L (2014). Rewiring cell polarity signaling in cancer. Oncogene 34, 939–950.

Hao Y, Du Q, Chen X, Zheng Z, Balsbaugh JL, Maitra S, Shabanowitz J, Hunt DF, Macara IG (2010). Par3 controls epithelial spindle orientation by aPKC-mediated phosphorylation of apical pins. Curr Biol 20, 1809–1818.

Hogan C, Dupre-Crochet S, Norman M, Kajita M, Zimmermann C, Pelling AE, Piddini E, Baena-Lopez LA, Vincent JP, Itoh Y, *et al.* (2009). Characterization of the interface between normal and transformed epithelial cells. Nat Cell Biol 11, 460–467.

Iden S, van Riel Wilhelmina E, Schäfer R, Song J-Y, Hirose T, Ohno S, Collard John G (2012). Tumor type-dependent function of the Par3 polarity protein in skin tumorigenesis. Cancer Cell 22, 389–403.

Jaffe AB, Kaji N, Durgan J, Hall A (2008). Cdc42 controls spindle orientation to position the apical surface during epithelial morphogenesis. J Cell Biol 183, 625–633.

Justilien V, Fields AP (2009). Ect2 links the PKCiota-Par6alpha complex to Rac1 activation and cellular transformation. Oncogene 28, 3597–3607.

Justilien V, Walsh MP, Ali SA, Thompson EA, Murray NR, Fields AP (2014). The PRKCI and SOX2 oncogenes are coamplified and cooperate to activate Hedgehog signaling in lung squamous cell carcinoma. Cancer Cell 25, 139–151.

Kadono Y, Okada Y, Namiki M, Seiki M, Sato H (1998). Transformation of epithelial Madin-Darby canine kidney cells with p60(v-src) induces expression of membrane-type 1 matrix metalloproteinase and invasiveness. Cancer Res 58, 2240–2244.

Kato S, Akimoto K, Nagashima Y, Ishiguro H, Kubota K, Kobayashi N, Hosono K, Watanabe S, Sekino Y, Sato T, *et al.* (2013). aPKClambda/iota is a beneficial prognostic marker for pancreatic neoplasms. Pancreatology 13, 360–368.

Kojima Y, Akimoto K, Nagashima Y, Ishiguro H, Shirai S, Chishima T, Ichikawa Y, Ishikawa T, Sasaki T, Kubota Y, *et al.* (2008). The overexpression and altered localization of the atypical protein kinase C lambda/iota in breast cancer correlates with the pathologic type of these tumors. Hum Pathol 39, 824–831.

Langzam L, Koren R, Gal R, Kugel V, Paz A, Farkas A, Sampson SR (2001). Patterns of protein kinase C isoenzyme expression in transitional cell carcinoma of bladder. Relation to degree of malignancy. Am J Clin Pathol 116, 377–385.
Levchenko T, Bratt A, Arbiser JL, Holmgren L (2004). Angiomotin expression promotes hemangioendothelioma invasion. Oncogene 23, 1469–1473.
Lin YM, Su CC, Su WW, Hwang JM, Hsu HH, Tsai CH, Wang YC, Tsai FJ, Huang CY, Liu JY, Chen LM (2012). Expression of protein kinase C isoforms in cancerous breast tissue and adjacent normal breast tissue. Chin J Physiol 55, 55–61.
Linch M, Sanz-Garcia M, Rosse C, Riou P, Peel N, Madsen CD, Sahai E, Downward J, Khwaja A, Dillon C, *et al.* (2014). Regulation of polarized morphogenesis by protein kinase C iota in oncogenic epithelial spheroids. Carcinogenesis 35, 396–406.
Ma Y, Yang Y, Wang F, Wei Q, Qin H (2014). Hippo-YAP signaling pathway: a new paradigm for cancer therapy. Int J Cancer 2014, doi: 10.1002/ijc.29073.
Martin-Belmonte F, Perez-Moreno M (2011). Epithelial cell polarity, stem cells and cancer. Nat Rev Cancer 12, 23–38.
McCaffrey Luke M, Montalbano J, Mihai C, Ian Macara G (2012). Loss of the Par3 polarity protein promotes breast tumorigenesis and metastasis. Cancer Cell 22, 601–614.
Moleirinho S, Guerrant W, Kissil JL (2014). The angiomotins—from discovery to function. FEBS Lett 588, 2693–2703.
Namdarian B, Wong E, Galea R, Pedersen J, Chin X, Speirs R, Humbert PO, Costello AJ, Corcoran NM, Hovens CM (2013). Loss of APKC expression independently predicts tumor recurrence in superficial bladder cancers. Urol Oncol 31, 649–655.
Nishimura T, Kaibuchi K (2007). Numb controls integrin endocytosis for directional cell migration with aPKC and PAR-3. Dev Cell 13, 15–28.
Paget JA, Restall IJ, Daneshmand M, Mersereau JA, Simard MA, Parolin D AE, Lavictoire SJ, Amin MS, Islam S, Lorimer IAJ (2011). Repression of cancer cell senescence by PKCι. Oncogene 31, 3584–3596.
Paramasivam M, Sarkeshik A, Yates JR 3rd, Fernandes MJ, McCollum D (2011). Angiomotin family proteins are novel activators of the LATS2 kinase tumor suppressor. Mol Biol Cell 22, 3725–3733.
Paul A, Gunewardena S, Stecklein SR, Saha B, Parelkar N, Danley M, Rajendran G, Home P, Ray S, Jokar I, *et al.* (2014). PKClambda/iota signaling promotes triple-negative breast cancer growth and metastasis. Cell Death Differ 21, 1469–1481.
Piccolo S, Dupont S, Cordenonsi M (2014). The biology of YAP/TAZ: hippo signaling and beyond. Physiol Rev 94, 1287–1312.
Pu YS, Huang CY, Chen JY, Kang WY, Lin YC, Shiu YS, Chuang SJ, Yu HJ, Lai MK, Tsai YC, *et al.* (2012). Down-regulation of PKCzeta in renal cell carcinoma and its clinicopathological implications. J Biomed Sci 19, 39.
Puliafito A, Hufnagel L, Neveu P, Streichan S, Sigal A, Fygenson DK, Shraiman BI (2012). Collective and single cell behavior in epithelial contact inhibition. Proc Natl Acad Sci USA 109, 739–744.
Regala RP, Weems C, Jamieson L, Khoor A, Edell ES, Lohse CM, Fields AP (2005). Atypical protein kinase C iota is an oncogene in human non-small cell lung cancer. Cancer Res 65, 8905–8911.
Romano D, Matallanas D, Frederick DT, Flaherty KT, Kolch W (2014). One Hippo and many masters: differential regulation of the Hippo pathway in cancer. Biochem Soc Trans 42, 816–821.
Sakurai A, Matsuda M, Kiyokawa E (2012). Activated Ras protein accelerates cell cycle progression to perturb Madin-Darby canine kidney cystogenesis. J Biol Chem 287, 31703–31711.
Sanz L, Sanchez P, Lallena MJ, Diaz-Meco MT, Moscat J (1999). The interaction of p62 with RIP links the atypical PKCs to NF-kappaB activation. EMBO J 18, 3044–3053.
Schlegelmilch K, Mohseni M, Kirak O, Pruszak J, Rodriguez JR, Zhou D, Kreger BT, Vasioukhin V, Avruch J, Brummelkamp TR, Camargo FD (2011). Yap1 acts downstream of alpha-catenin to control epidermal proliferation. Cell 144, 782–795.
Smith CA, Lau KM, Rahmani Z, Dho SE, Brothers G, She YM, Berry DM, Bonneil E, Thibault P, Schweisguth F, *et al.* (2007). aPKC-mediated phosphorylation regulates asymmetric membrane localization of the cell fate determinant Numb. EMBO J 26, 468–480.
Sotillos S, Diaz-Meco MT, Caminero E, Moscat J, Campuzano S (2004). DaPKC-dependent phosphorylation of Crumbs is required for epithelial cell polarity in Drosophila. J Cell Biol 166, 549–557.
Standaert ML, Bandyopadhyay G, Perez L, Price D, Galloway L, Poklepovic A, Sajan MP, Cenni V, Sirri A, Moscat J, *et al.* (1999). Insulin activates protein kinases C-zeta and C-lambda by an autophosphorylation-dependent mechanism and stimulates their translocation to GLUT4 vesicles and other membrane fractions in rat adipocytes. J Biol Chem 274, 25308–25316.
Toyli M, Rosberg-Kulha L, Capra J, Vuoristo J, Eskelinen S (2010). Different responses in transformation of MDCK cells in 2D and 3D culture by v-Src as revealed by microarray techniques, RT-PCR and functional assays. Lab Invest 90, 915–928.
Tsai JH, Hsieh YS, Kuo SJ, Chen ST, Yu SY, Huang CY, Chang AC, Wang YW, Tsai MT, Liu JY (2000). Alteration in the expression of protein kinase C isoforms in human hepatocellular carcinoma. Cancer Lett 161, 171–175.
Varelas X, Samavarchi-Tehrani P, Narimatsu M, Weiss A, Cockburn K, Larsen BG, Rossant J, Wrana JL (2010). The Crumbs complex couples cell density sensing to Hippo-dependent control of the TGF-beta-SMAD pathway. Dev Cell 19, 831–844.
Varelas X, Wrana JL (2012). Coordinating developmental signaling: novel roles for the Hippo pathway. Trends Cell Biol 22, 88–96.
Yang CC, Graves HK, Moya IM, Tao C, Hamaratoglu F, Gladden AB, Halder G (2015). Differential regulation of the Hippo pathway by adherens junctions and apical-basal cell polarity modules. Proc Natl Acad Sci USA 112, 1785–1790.
Yang YL, Chu JY, Luo ML, Wu YP, Zhang Y, Feng YB, Shi ZZ, Xu X, Han YL, Cai Y, *et al.* (2008). Amplification of PRKCI, located in 3q26, is associated with lymph node metastasis in esophageal squamous cell carcinoma. Genes Chromosomes Cancer 47, 127–136.
Yao S, Bee A, Brewer D, Dodson A, Beesley C, Ke Y, Ambroisine L, Fisher G, Moller H, Dickinson T, *et al.* (2010). PRKC-zeta expression promotes the aggressive phenotype of human prostate cancer cells and is a novel target for therapeutic intervention. Genes Cancer 1, 444–464.
Yao S, Ireland SJ, Bee A, Beesley C, Forootan SS, Dodson A, Dickinson T, Gerard P, Lian LY, Risk JM, *et al.* (2012). Splice variant PRKC-zeta(-PrC) is a novel biomarker of human prostate cancer. Br J Cancer 107, 388–399.
Yi C, Shen Z, Stemmer-Rachamimov A, Dawany N, Troutman S, Showe LC, Liu Q, Shimono A, Sudol M, Holmgren L, *et al.* (2013). The p130 isoform of angiomotin is required for Yap-mediated hepatic epithelial cell proliferation and tumorigenesis. Sci Signal 6, ra77.
Yin F, Yu J, Zheng Y, Chen Q, Zhang N, Pan D (2013). Spatial organization of Hippo signaling at the plasma membrane mediated by the tumor suppressor Merlin/NF2. Cell 154, 1342–1355.
Yin J, Liu Z, Li H, Sun J, Chang X, Liu J, He S, Li B (2014). Association of PKCzeta expression with clinicopathological characteristics of breast cancer. PLoS One 9, e90811.
Yu FX, Guan KL (2013). The Hippo pathway: regulators and regulations. Genes Dev 27, 355–371.
Zhang H, Liu G, Dziubinski M, Yang Z, Ethier SP, Wu G (2008). Comprehensive analysis of oncogenic effects of PIK3CA mutations in human mammary epithelial cells. Breast Cancer Res Treat 112, 217–227.
Zhao B, Li L, Lu Q, Wang LH, Liu CY, Lei Q, Guan KL (2011). Angiomotin is a novel Hippo pathway component that inhibits YAP oncoprotein. Genes Dev 25, 51–63.